Cell Reports

Article

DRD1 signaling modulates TrkB turnover and BDNF sensitivity in direct pathway striatal medium spiny neurons

Graphical abstract

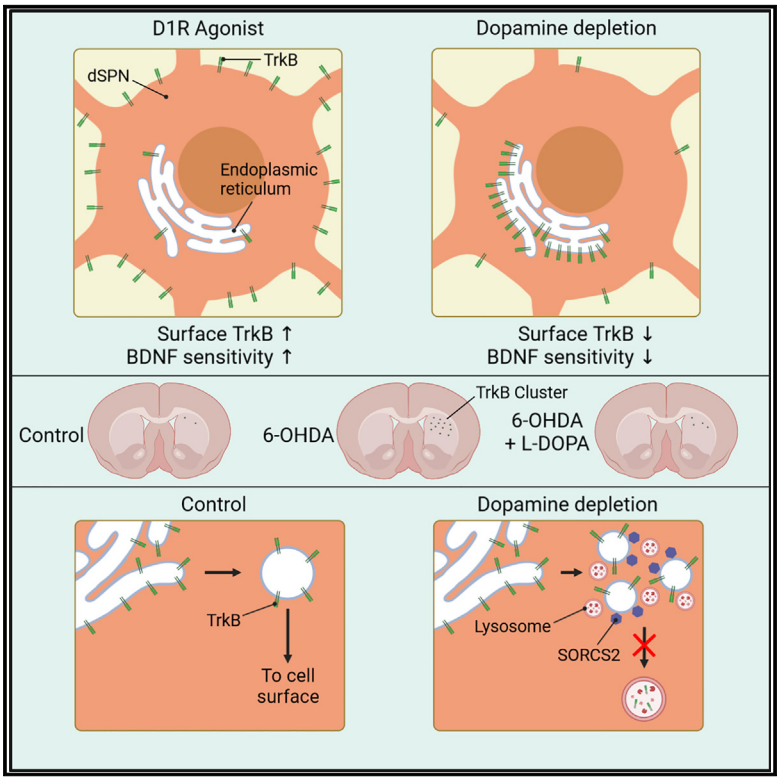

Highlights

- Dopamine receptor-1 activation induces TrkB cell-surface expression in striatal neurons
- Dopaminergic deficits cause TrkB accumulation and clustering in the ER
- TrkB clusters colocalize with cargo receptor SORCS-2 in direct pathway striatal neurons
- Intracellular TrkB clusters fail to fuse with lysosomes after dopamine depletion

Authors

Thomas Andreska, Patrick Lüningschrör, Daniel Wolf, ..., Chi Wang Ip, Christian Stigloher, Michael Sendtner

Correspondence

sendtner_m@ukw.de

In brief

Andreska et al. show that TrkB cell-surface expression in striatal direct pathway neurons is controlled by dopamine receptor-1 signaling, thus regulating the sensitivity for BDNF signaling from cortical afferents. In dopamine-depleted neurons, intracellular TrkB is sequestered in clusters that are prominent in postmortem brain from patients with PD.

Andreska et al., 2023, Cell Reports *42*, 112575
June 27, 2023
https://doi.org/10.1016/j.celrep.2023.112575

CellPress

Cell Reports

CellPress
OPEN ACCESS

Article

DRD1 signaling modulates TrkB turnover and BDNF sensitivity in direct pathway striatal medium spiny neurons

Thomas Andreska,[1] Patrick Lüningschrör,[1] Daniel Wolf,[1] Rhonda L. McFleder,[2] Maurilyn Ayon-Olivas,[1] Marta Rattka,[2] Christine Drechsler,[3,10] Veronika Perschin,[4] Robert Blum,[2] Sarah Aufmkolk,[5,6] Noelia Granado,[7,8] Rosario Moratalla,[7,8] Markus Sauer,[5] Camelia Monoranu,[9] Jens Volkmann,[2] Chi Wang Ip,[2] Christian Stigloher,[4] and Michael Sendtner[1,11,*]

[1]Institute of Clinical Neurobiology, University Hospital Wuerzburg, 97078 Wuerzburg, Germany
[2]Department of Neurology, University Hospital Wuerzburg, 97080 Wuerzburg, Germany
[3]Department of Microbiology, Biocenter, Julius-Maximilians-University Wuerzburg, 97074 Wuerzburg, Germany
[4]Imaging Core Facility of the Biocenter, Julius-Maximilians-University Wuerzburg, 97074 Wuerzburg, Germany
[5]Department of Biotechnology and Biophysics, Julius-Maximilians-University Wuerzburg, 97074 Wuerzburg, Germany
[6]Department of Genetics, Harvard Medical School, Boston, MA 02115, USA
[7]Instituto Cajal, Consejo Superior de Investigaciones Científicas (CSIC), Madrid, Spain
[8]CIBERNED, Instituto de Salud Carlos III, 28002 Madrid, Spain
[9]Department for Neuropathology, Julius-Maximilians-University Wuerzburg, 97080 Wuerzburg, Germany
[10]Present address: The Healthcare Business of Merck KGaA, 64293 Darmstadt, Germany
[11]Lead contact
*Correspondence: sendtner_m@ukw.de
https://doi.org/10.1016/j.celrep.2023.112575

SUMMARY

Disturbed motor control is a hallmark of Parkinson's disease (PD). Cortico-striatal synapses play a central role in motor learning and adaption, and brain-derived neurotrophic factor (BDNF) from cortico-striatal afferents modulates their plasticity via TrkB in striatal medium spiny projection neurons (SPNs). We studied the role of dopamine in modulating the sensitivity of direct pathway SPNs (dSPNs) to BDNF in cultures of fluorescence-activated cell sorting (FACS)-enriched D1-expressing SPNs and 6-hydroxydopamine (6-OHDA)-treated rats. DRD1 activation causes enhanced TrkB translocation to the cell surface and increased sensitivity for BDNF. In contrast, dopamine depletion in cultured dSPN neurons, 6-OHDA-treated rats, and postmortem brain of patients with PD reduces BDNF responsiveness and causes formation of intracellular TrkB clusters. These clusters associate with sortilin related VPS10 domain containing receptor 2 (SORCS-2) in multivesicular-like structures, which apparently protects them from lysosomal degradation. Thus, impaired TrkB processing might contribute to disturbed motor function in PD.

INTRODUCTION

The striatum is a central part of the basal ganglia circuitry for motor control and learning.[1–6] Motor learning depends on "bidirectional" synaptic modulation of cortico-striatal synapses on medium spiny projection neurons (SPNs).[4,5,7–9] Cortico-striatal synaptic plasticity is not only required for normal motor learning, but alterations in synaptic strength along with progressive decrease in striatal dopamine (DA) contribute to motor dysfunction in Parkinson's disease (PD).[5,10–15] Dopaminergic input to the striatum has a strong modulatory effect on cortico-striatal synaptic plasticity.[4,5,10,11,13–20] Striatal SPNs are sensitive to DA via the G-protein-coupled receptors (GPCRs) dopamine receptor D1 (DRD1) in direct pathway SPNs (dSPNs) and DRD2 in indirect pathway SPNs (iSPNs).[4,21] DRD1 activation enhances glutamatergic transmission through the NMDA receptor (NMDAR) and could therefore contribute to LTP facilitation at cortico-striatal synapses.[5,22,23] In PD, this mode of plasticity is altered: dSPNs switch from long-term potentiation (LTP) to long-term depression (LTD) when DRD1 activation is absent.[5,24] However, the mechanism behind this altered plasticity is unknown.

Cortico-striatal LTP depends on simultaneous activation of NMDAR, dopaminergic signaling via $G_{\alpha s/olf}$-protein-coupled receptors (DRD1),[25] and activation of TrkB.[4,6] Blockade of BDNF/TrkB signaling abolishes cortico-striatal LTP, which underlines the importance of BDNF/TrkB interaction in striatal neurons.[26–28] However, the mechanisms of altered BDNF/TrkB signaling in dSPNs and iSPNs after DA depletion are still obscure. BDNF levels are not reduced in striatum and cortex of PD animal models.[29] Similarly, no reduction of BDNF was observed in the frontal cortex of postmortem brain of patients with PD but rather in caudate nucleus and putamen.[30] Cortex and midbrain are the main sources of afferent BDNF input

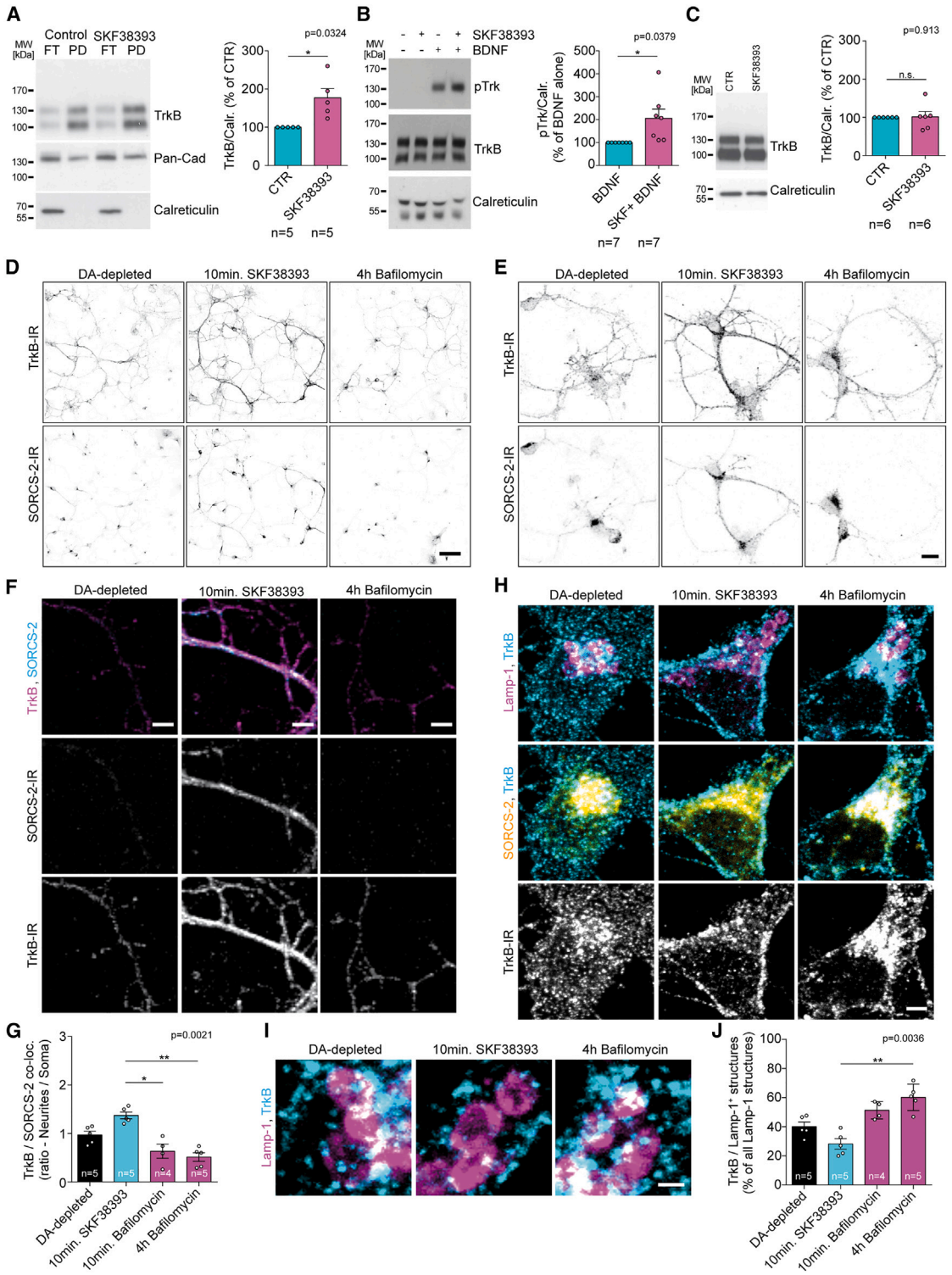

Figure 1. DRD1 promotes dSPN sensitivity for BDNF by increasing TrkB surface expression

(A) Surface biotinylation assay of FACS-enriched dSPNs at days *in vitro* (DIV) 6–7. TrkB surface expression is increased after 10-min stimulation of DRD1 with 2 μM SKF38393. Quantification of TrkB cell-surface expression reveals a significant increase after DRD1 stimulation ($p = 0.0324$; data are shown as mean ± SEM in % of untreated control; n = 5/condition; one-sample t test).

(B) Western blot showing pTrk induction in FACS dSPNs at DIV6–7. No pTrk is evident at control conditions or with SKF38393 alone (lanes 1 and 2). Incubation with 10 ng/ml BDNF for 5 min induces Trk phosphorylation (lane 3). Preincubation with 2 μM SKF38393 for 5 min followed by 10 ng/ml BDNF for another 5 min

(legend continued on next page)

toward the striatum.[28,31–33] Reduced striatal BDNF levels might be explained by a progressive loss of BDNF from nigrostriatal afferents.[30,34–36] However, striatal BDNF has been shown to be much more prominent in cortex-derived glutamatergic rather than dopaminergic terminals.[33] These cortico-striatal fibers are still intact when nigrostriatal BDNF supply is lost. Consequently, altered SPN sensitivity for BDNF could be a major pathological mechanism in PD.

Target cell sensitivity for BDNF relies on cell-surface localization of TrkB, a mechanism that depends on cyclic AMP (cAMP).[37] In dSPNs, cAMP levels are elevated via DRD1-$G_{\alpha s}$-mediated stimulation of adenylyl cyclase 5 (AC5).[4,21,22] Here, we provide evidence that $G_{\alpha s}$-coupled DRD1 activation increases TrkB cell-surface expression and thereby modulates sensitivity for BDNF. Conversely, absence of DA in fluorescence-activated cell sorting (FACS)-enriched dSPN cultures *in vitro*, in hemiparkinsonian 6-OHDA rat brain, and postmortem brain of patients with PD results in TrkB mislocalization in large multivesicular body-like perinuclear clusters in dSPNs. These TrkB clusters are closely associated with SORCS-2, a cargo receptor required for surface export of transmembrane proteins, including TrkB, which also links cargo to the retromer complex and prevents lysosomal degradation.[38–40] Importantly, the intracellular TrkB clusters showed impaired ability to enter lysosomal degradation. Thus, the absence of striatal DA leads to reduced TrkB cell-surface expression in DRD1-expressing dSPNs that is accompanied by abnormal intracellular processing of TrkB and reduced sensitivity to BDNF from cortico-striatal afferents.

This indicates that DA is essential for intracellular processing of TrkB in dSPNs, and that restoration of this process might be beneficial for PD treatment.

RESULTS

DRD1 activation in dSPNs increases TrkB cell-surface translocation and BDNF sensitivity

Cortico-striatal projections from the motor cortex express relatively high levels of BDNF.[3,41–43] These afferents target dendritic spines of SPNs that also receive dopaminergic input from the midbrain.[31] However, co-staining of BDNF together with VGlut1 and tyrosine hydroxylase (TH) on mouse striatal tissue revealed that striatal BDNF is more prominent in VGlut1-positive cortex-derived rather than dopaminergic midbrain-derived terminals[33] (Figure S1). To test whether activation of the $G_{\alpha s/olf}$-coupled receptor DRD1 in dSPNs modulates BDNF responsiveness, we developed a FACS-based technique for enrichment of dSPNs *in vitro* using DRD1-Td-Tomato reporter mice[44] (Figure S2A). Enriched dSPNs were cultured for 7 days before treatment with the DRD1 receptor agonist SKF38393 (2 μM) for a period of 10 min. Based on previous analyses in early cortical neurons, we hypothesized that a significant proportion of TrkB is located within the endoplasmic reticulum (ER)[45] and shifted to the cell surface by increased intracellular cAMP.[37] To test whether this effect also occurs in striatal dSPNs after activation of DRD1, which enhances cAMP levels,[4,21] we performed surface biotinylation of TrkB in the presence or absence of SKF38393. DRD1 activation with SKF38393 led to a significant increase in TrkB biotinylation on the cell surface (Figure 1A). To independently confirm this result, we stained TrkB on the cell surface of living cells using an antibody against the extracellular domain of TrkB. We compared TrkB cell-surface expression under DA-depleted conditions and after stimulation of DRD1 using an independent agonist, SKF81297. A third cohort of FACS dSPNs was stimulated with oxotremorine M, an agonist of the $G_{\alpha i}$-coupled M4R

causes elevation of pTrk (lane 4). Quantification of pTrk induction by BDNF reveals a significant increase after stimulation of DRD1 ($p = 0.0379$; data are shown as mean ± SEM in % of pTrk levels after BDNF stimulation alone; n = 7/condition; one-sample t test).

(C) Western blot analyses of total TrkB protein in whole-cell lysates of control or SKF38393-treated dSPNs used for surface biotinylation. Quantification of total TrkB-full-length (TrkB-FL) (130 kDa) reveals no change in total TrkB after DRD1 stimulation ($p = 0.9130$; data are shown as mean ± SEM in % of untreated control; n = 6/condition; one-sample t test).

(D and E) TrkB-IR and SORCS-2-immunoreactivity (IR) in dSPNs in the absence of dopamine, 10 min of 2 μM SKF38393, and 4 h of 100 nM bafilomycin to block lysosomal degradation. Higher magnification in (E) reveals perinuclear cluster formation of TrkB and SORCS-2 in the absence of DRD1 activity. Activation of DRD1 for 10 min causes increased TrkB and SORCS-2-IR in peripheral neurites. Blockade of lysosomal degradation by bafilomycin reduces TrkB and SORCS-2-IR in peripheral neurites and leads to perinuclear cluster formation of both receptors.

(F) High-magnification images of peripheral neurites from cultures depicted in (D) and (E). TrkB and SORCS-2-IR are sparse under DA-depleted conditions and reveal an increase in IR intensity after 10 min. DRD1 activation using SKF38393. Bafilomycin treatment for 4 h causes further reduction of SORCS-2-IR in peripheral neurites.

(G) Quantification of the ratio of TrkB/SORCS-2 co-localization in neurites versus cell body (depicted in F and H) reveals increased colocalization in peripheral neurites after DRD1 activation and significant somatic enrichment after bafilomycin treatment ($p = 0.0021$; data are shown as mean ± SEM as co-localization ratio between TrkB/SORCS-2 in neurites versus soma; n = 4 independent replicates for 10 min of bafilomycin and n = 5/other condition; ≥5 cells were analyzed per replicate; one-way ANOVA, Kruskal-Wallis test).

(H) High-magnification confocal microscopy reveals perinuclear TrkB clusters associated with Lamp-1-positive structures and SORCS-2 in the absence of DRD1 activity. Stimulation of DRD1 for 10 min causes TrkB-IR at cell membrane positions, less association with Lamp-1 structures, and SORCS-2 at perinuclear sites. Blockade of lysosomal acidification and degradation by bafilomycin results in huge perinuclear TrkB cluster formation, association with Lamp-1-positive structures, and significant overlap with a SORCS-2 cluster at the same position.

(I) High-magnification images of perinuclear TrkB/Lamp-1-positive structures shown in (H).

(J) Quantification of TrkB/Lamp-1-positive structures reveals a decrease after DRD1 activation compared with DA-depleted control. TrkB association with Lamp-1 structures is significantly increased after 4-h incubation with bafilomycin ($p = 0.0036$; data are shown as mean ± SEM in % of all Lamp-1-positive structures; n = 4 independent replicates for "10 min. Bafilomycin" and n = 5/other condition; ≥5 cells were analyzed per replicate; one-way ANOVA, Kruskal-Wallis test).

$p > 0.05$; *$p \leq 0.05$; **$p \leq 0.01$; ***$p \leq 0.001$; ****$p \leq 0.0001$. Scale bars: 50 μm (D); 10 μm (E); 5 μm (F); 2.5 μm (H); 1 μm (I). FT, flowthrough; PD, pull-down. See also Figure S2.

that should reduce cAMP levels and therefore reduce TrkB cell-surface expression.[46] We observed increased TrkB-IR on the cell surface of FACS dSPNs after stimulation of DRD1 with SKF81297 and reduced TrkB-IR after activation of M4R with oxotremorine M, compared with DA-depleted control condition (Figure S2B). Increased TrkB cell-surface expression could result in higher sensitivity for BDNF compared with DA-depleted dSPNs. Indeed, BDNF treatment of dSPNs, preincubated with the DRD1 receptor agonist for 5 min, resulted in a significant increase in TrkB activation compared with DA-depleted dSPNs (Figure 1B). Total TrkB protein levels remained unchanged during this 10-min period of stimulation, excluding the possibility that *de novo* synthesis of TrkB is responsible for increased pTrk levels after BDNF stimulation (Figure 1C). The enrichment of biotinylated TrkB provides evidence that DRD1 activation shifts TrkB from intracellular compartments to the cell surface, thus increasing the sensitivity of dSPNs for BDNF from cortical afferents.

To investigate the subcellular distribution of TrkB in more detail, we stained dSPNs for TrkB distribution together with SORCS-2, a member of the VPS-10P family of cargo receptors known to interact with TrkB and mediate its translocation to the dendritic cell surface.[38,40,47–51] Members of the VPS-10P family of cargo adapters also modulate targeting of proteins to recycling or to lysosomal degradation.[52,53] Thus, SORCS2 is a strong candidate for targeting intracellular TrkB to the cell surface rather than to the lysosomal degradation pathway.[54] In DA-depleted dSPNs, we observed moderate TrkB and SORCS-2-IR in neurites (Figures 1D–1G, left). However, stimulation of DRD1 with SKF38393 for 10 min increased TrkB and SORCS-2-IR in peripheral neurites (Figures 1D–1G, middle), which is in line with previous reports showing SORCS-2-mediated transport of TrkB to the dendritic surface.[38] In the cell body, we observed formation of intracellular TrkB clusters that colocalized with SORCS-2 under conditions of DA depletion (Figures 1E and 1H, left). These clusters were surrounded by Lamp-1-positive structures of which ~38% revealed TrkB-IR-positive punctae either in the lumen or the membrane (Figures 1H, 1I, left, and 1J). DRD1 stimulation increased TrkB-IR on the cell surface (Figure 1H, middle) and reduced TrkB-IR association with Lamp-1-positive structures (Figures 1H and 1I, middle) to ~25% compared with ~38% in DA-depleted control (Figure 1J).

Because impaired autophagy-lysosomal pathways represent a major pathology in PD, besides loss of DA,[55] we included another condition in which lysosomal degradation was blocked with 100 nM bafilomycin. Under these conditions, TrkB and SORCS-2-IR were reduced in peripheral neurites (Figures 1D–1F, right). Quantification of TrkB/SORCS-2 co-localization confirmed a reduction of both receptors in neurites and an increase in cell bodies after 10 min or 4 h of bafilomycin treatment (Figure 1G). This increase in somatic overlap of TrkB and SORCS-2 was accompanied by massive perinuclear cluster formation of both proteins (Figures 1E and 1H, right). These clusters revealed a close association with Lamp-1-positive structures, of which ~52% overlapped with TrkB-IR after 10 min and ~60% after 4 h of bafilomycin treatment (Figures 1H, 1I, right, and 1J).

Taken together, these *in vitro* data indicate that activation of DRD1 in dSPNs promotes translocation of TrkB to the cell surface, which involves SORCS-2. At the same time, translocation of TrkB to lysosomes and receptor degradation apparently decreases. However, reduced DRD1 activity results in perinuclear TrkB/SORCS-2 clusters in some dSPNs. These clusters are closely associated with lysosomal structures, probably by reduced entry into lysosomal degradation pathways. Blockade of lysosomal degradation exaggerates this effect, resulting in larger clusters with increased association to Lamp-1-positive structures.

6-OHDA treatment causes TrkB cluster formation in hemiparkinsonian rats

The effects of DRD1 agonists on TrkB cell-surface translocation indicate that dopaminergic afferents modulate dSPN sensitivity for BDNF. This could contribute to pathological alterations in cortico-striatal plasticity in PD.[4,12,56] Therefore, we investigated the subcellular distribution of TrkB in striatal SPNs of hemiparkinsonian 6-OHDA rats.[57–59] Because striatal BDNF is supplied via cortico-striatal and nigrostriatal afferents,[31,41] loss of nigrostriatal BDNF following 6-OHDA-mediated elimination of dopaminergic neurons could induce compensatory BDNF upregulation in cortico-striatal pathways. In order to study potential alterations in cortical BDNF expression on the cellular level, we performed immunohistochemistry (IHC) and compared the lesioned and unlesioned hemispheres. We did not observe a difference in BDNF-IR within cortical neurons of layer II/III between the intact and DA-depleted hemisphere at three different time points after inducing the 6-OHDA lesion (Figure S3). We focused on the dorsolateral striatum, which receives dense glutamatergic and BDNF-positive afferents from motor cortex.[2,3] 6-OHDA injection into the medial forebrain bundle[60] resulted in virtually complete depletion of TH-positive fibers in the lesioned striatal hemisphere (Figure 2A). Large TrkB cluster-like structures became apparent on the DA-depleted, but not the control side even at low magnification (Figure 2B). TrkB clusters were located intracellularly at a perinuclear position (Figure 2C), closely resembling our *in vitro* observations in FACS dSPNs (Figure 1H). Furthermore, the overall TrkB-IR intensity outside cell bodies in dendritic trees appeared reduced in the DA-depleted hemisphere (Figures 2B and 2C). The density of these TrkB-positive clusters did not change significantly between 2 weeks and 4 months after 6-OHDA lesion (Figure 2D). However, the diameter of the TrkB clusters alone (Figure 2E) or after normalization to the size of the nucleus of the same cell (Figure 2F) increased significantly between 2 and 4 or 16 weeks, respectively.

We next tested whether TrkB clusters specifically occur in SPNs, and we performed co-staining of TrkB with DARPP-32, a cytosolic protein expressed in striatal SPNs. A subpopulation of DARPP-32-positive striatal SPNs revealed TrkB clusters (Figure 2G). These TrkB clusters did not overlap with DARPP-32-IR in the cytosol because DARPP-32-positive cytosolic IR seems to be spared by TrkB accumulation (Figure 2G detail). This suggests that TrkB is engulfed by at least one membrane in an intracellular compartment.

To test the specificity of this TrkB staining, we used an independent antiserum against the complete extracellular domain of TrkB. This TrkB antiserum (AF1494) stained the same clusters as the 07–225 antiserum that is directed against an 18-amino

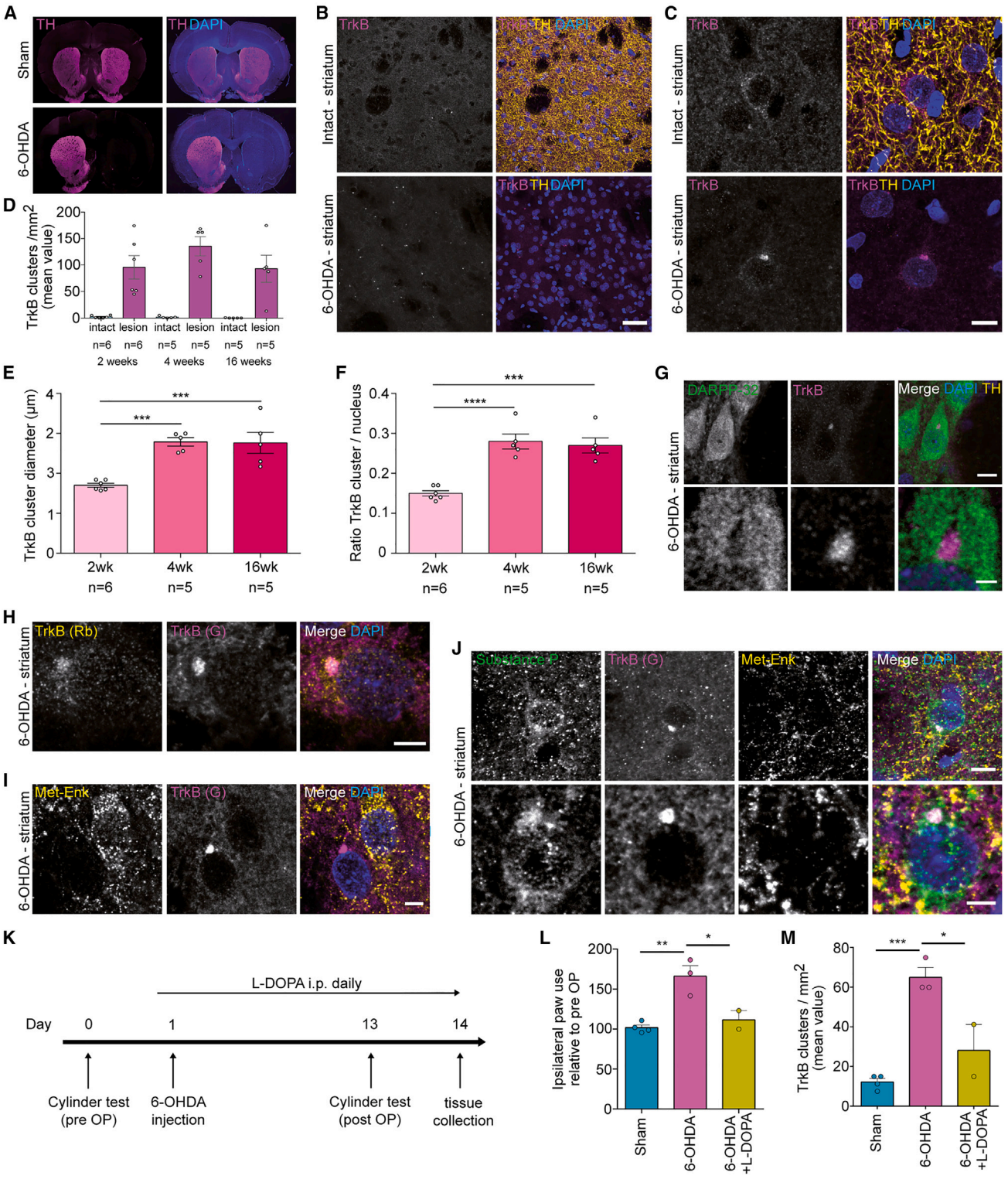

Figure 2. DA depletion by 6-OHDA leads to TrkB cluster formation in striatal SPNs

(A) IHC image showing tyrosine hydroxylase (TH)-IR in coronal sections of sham versus unilateral 6-OHDA-lesioned rat brain.

(B) Higher magnification IHC image showing dorsolateral striatum of intact and DA-depleted hemisphere, indicated by absence of TH-IR. TrkB-IR reveals cluster formation of the receptor in absence of DA.

(C) High-magnification image revealing perinuclear accumulation of TrkB in the absence of DA.

(legend continued on next page)

acid domain of the extracellular domain (Figure 2H). The specificity of both TrkB antisera was also tested in TrkB knockout mice. TrkB-IR signals were absent in brains of P5 *TrkB*$^{-/-}$ (Ntrk-Rohrer) mice (Figures S4A–S4F) and striatal protein extracts of *TrkB*$^{-/-}$ animals, as revealed by western blot (WB) analyses (Figures S4G and S4H).

We next investigated whether TrkB cluster formation is different in dSPNs versus iSPNs. To validate marker proteins for SPN identification, we used established GFP-reporter mouse models[61] for double staining with Met-Enkephalin, a specific marker for iSPNs (Figures S5A and S5B). After confirming the specific expression of Met-Enkephalin in iSPNs (Figure S5C), we stained brain sections from hemiparkinsonian rats and noticed an upregulation of Met-Enk-IR in iSPNs of the DA-depleted striatum (Figure S5D), confirming earlier reports.[62–64] However, TrkB accumulations were observed only in Met-Enkephalin-negative cells, indicating that they occur in dSPNs (Figure 2I). In order to directly confirm dSPN identity, we co-stained for substance P, which is specifically expressed in dSPNs,[10] together with TrkB and Met-Enkephalin (Figure 2J). We observed that TrkB clusters exclusively occurred in SPNs that express substance P but lack Met-Enkephalin expression, identifying them as dSPNs (Figure 2J). This finding is supported by earlier observations showing that under conditions of DA depletion, substance P is downregulated in dSPNs, whereas Met-Enkephalin is upregulated in iSPNs[65] (cf. Figure S5D). Together these findings exclude the possibility of TrkB clustering in iSPNs that downregulate Met-Enkephalin expression.

We then investigated whether the formation of TrkB-positive clusters can be rescued by L-DOPA treatment. Recent studies with slice preparations from 6-OHDA-treated mice demonstrated that defects in LTP formation that occurred at corticostriatal synapses after DA depletion could be rescued by L-DOPA treatment.[19] Drd1-td-Tomato reporter mice were injected unilaterally with 6-OHDA and treated daily with intraperitoneal injection of L-DOPA and benserazide for a period of 2 weeks (Figure 2K). Success of the 6-OHDA treatment was tested by staining of brain sections against TH (Figure S6A). Ipsilateral paw use in the cylinder test was investigated as a behavioral readout for motor dysfunction after 6-OHDA treatment. These analyses showed that the rescue with L-DOPA treatment was successful on the behavioral level (Figure 2L). At day 14 after 6-OHDA injection, the mice were sacrificed, and TrkB clusters were investigated on the lesioned side. This analysis revealed that the number of TrkB clusters in DARPP-32-positive neurons was reduced from 64.9 to 28.2 clusters/mm^2 by daily L-DOPA treatment (Figures 2M and S6B). Due to the td-Tomato expression in dSPNs, the clusters could be investigated separately in the td-Tomato reporter-positive dSPNs and Met-Enkephalin-positive iSPNs. Similar as in 6-OHDA-treated rats, TrkB clusters were prominent in reporter-positive dSPNs, but not in Met-Enkephalin-positive iSPNs (Figure S6C).

To test whether TrkB clusters in DA-deprived 6-OHDA rat striatum occur as a result of decreased DRD1 activation, we investigated TrkB cluster formation in the striatum of *Drd1*$^{-/-}$ mice.[66] In these mice, perinuclear TrkB clusters could also be detected at enhanced numbers, compared with control *Drd1*$^{+/+}$ mice (Figure 3). However, compared with 6-OHDA-treated rats, the TrkB clusters appeared less frequent in *Drd1*$^{-/-}$ mice. Whereas approximately 100 clusters/mm^2 were detectable in 6-OHDA-treated rats, we detected only 12 clusters/mm^2 in *Drd1*$^{-/-}$ mice. In contrast with the 6-OHDA treatment, which induces an acute disruption of Drd1 signaling by DA depletion, the complete knockout of the Drd1 receptor may already cause alterations of BDNF/TrkB signaling during development that lead to different levels of compensation, which is possible because DRD1 KO mice show a wide spectrum of phenotypes, ranging from early lethality to close to healthy.[67,68]

Taken together, our *in vivo* data with hemiparkinsonian rats and *Drd1*$^{-/-}$ mice reveal perinuclear TrkB accumulation in striatal dSPNs after DA depletion, which is in line with our *in vitro* data using DA-depleted FACS-purified dSPNs.

TrkB clusters overlap with SORCS-2 and associate with lysosomal structures in hemiparkinsonian rat striatum

Previous work showed that TrkB is translocated to the cell surface from the ER.[45] For this reason, it is possible that TrkB is retained and accumulates in the ER of DA-deprived dSPNs in

(D) Quantification of TrkB cluster density in dorsolateral striatum comparing intact versus DA-depleted hemisphere. TrkB clusters appear only in DA-depleted striatum, and density does not significantly change over time between 2 weeks after lesion until 4 months after lesion. Data are shown as mean ± SEM; n = 6 for 2 weeks and n = 5/other condition; one-way ANOVA; Tukey multiple comparison test.
(E) Quantification of mean TrkB cluster diameter at 2, 4, and 16 weeks after lesion. Cluster diameter at 4 and 16 weeks is significantly increased compared with 2 weeks. Data are shown as mean ± SEM; n = 6 for 2 weeks and n = 5/other condition; one-way ANOVA, Tukey multiple comparison test.
(F) Quantification of the size ratio between TrkB cluster diameter and diameter of the nucleus of the same cell. TrkB/nucleus ratio significantly increases between 2 and 4 or 16 weeks, respectively. Data are shown as mean ± SEM; n = 6 for 2 weeks and n = 5/other condition; one-way ANOVA; Tukey multiple comparison test; $p > 0.05$; *$p \leq 0.05$; **$p \leq 0.01$; ***$p \leq 0.001$; ****$p \leq 0.0001$.
(G) TrkB clusters were exclusively identified in DARPP-32-positive striatal SPNs. Gap in cytoplasmic DARPP-32-IR indicates that TrkB accumulation is separated from the cytosol.
(H) Identification of intracellular TrkB clusters, using two independent antibodies against the N terminus of TrkB.
(I) High-magnification IHC image of DA-depleted rat striatum using Met-Enk-IR to identify iSPNs. TrkB clusters exclusively occur in cell bodies of Met-Enk-negative dSPNs. Neighboring iSPNs reveal no obvious somatic TrkB-IR pattern.
(J) High-magnification IHC image of DA-depleted rat striatum showing TrkB cluster in Met-Enk-negative and substance P-positive dSPNs.
(K) Timeline of 6-OHDA treatment for L-DOPA rescue.
(L) In the cylinder test, paw use ipsilateral to the 6-OHDA injection site was increased, and this effect was rescued by L-DOPA treatment. Data are shown as mean ± SEM; n = 4 for Sham, n = 3 for 6-OHDA, n = 2 for L-DOPA; one-way ANOVA; Tukey multiple comparison test; $p > 0.05$; *$p \leq 0.05$; **$p \leq 0.01$.
(M) TrkB clusters form rapidly in 6-OHDA-injected mice, and their number is reduced by daily L-DOPA treatment. Data are shown as mean ± SEM; n = 4 for Sham, n = 3 for 6-OHDA, n = 2 for L-DOPA; one-way ANOVA; Tukey multiple comparison test; $p > 0.05$; *$p \leq 0.05$; **$p \leq 0.01$; ***$p \leq 0.001$.
Scale bars: 50 μm (B); 10 μm (C; G, top; and J, top); 5 μm (H, top, I, and J, bottom); 2 μm (G, bottom). See also Figures S3–S6.

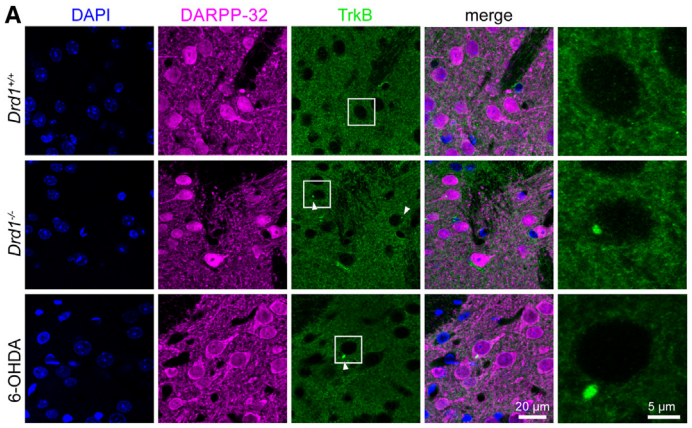

Figure 3. TrkB clusters in mouse striatum of Drd1-deficient mice

(A) Confocal microscopic images showing TrkB- and DARPP-32-IR in striatal sections, obtained from control mice (upper panel), *Drd1*-deficient mice (middle panel), and 6-OHDA-treated rats (lower panel). TrkB clusters occurred in DARPP-32-positive striatal SPNs of *Drd1*$^{-/-}$ mice. Scale bars: 20 µm (overview); 5 µm (detail).

(B) Quantification of TrkB clusters in control and *Drd1*$^{-/-}$ mice. Note that the TrkB clusters appeared at a lower frequency compared with 6-OHDA-lesioned rats (see Figure 2D). Each dot represents the mean value of an individual animal. Data are shown as mean ± SEM; n = 4/condition.

hemiparkinsonian rats. To test this hypothesis, we performed triple IHC staining of TrkB together with the ER markers Calreticulin and Calnexin. High-resolution structural illumination microscopy (SIM) revealed that TrkB clusters are surrounded by both ER markers without obvious signal overlap (Figure 4A). In addition, we used super-resolution direct stochastic optical reconstruction microscopy (dSTORM) and observed dense TrkB clusters surrounded by Calreticulin-IR (Figure 4B). Interestingly, Calreticulin-IR was sparse at the site of the TrkB cluster itself (Figure 4B detail). In addition, we stained for the Golgi markers GM130 and *trans*-Golgi network (TGN)-38, which both failed to show significant overlap with TrkB clusters (Figures S7A and S7B).

These observations raise the possibility that impaired SORCS-2-mediated cell-surface export of TrkB results in cluster formation. To test this hypothesis, we double-stained TrkB with SORCS-2 in 6-OHDA striatum. All TrkB clusters in dSPNs were positive for SORCS-2-IR, revealing almost complete absence of SORCS-2-IR in the remaining cell body (Figures 4C and 4D). Interestingly, SORCS-2-IR was distributed throughout the whole cell body in SPNs without TrkB clusters (Figure 4C). This observation points toward a mislocalization of TrkB, together with its associated cargo receptor SORCS-2 and confirms our initial observations made with FACS-enriched dSPNs *in vitro* (Figure 1H, left). The presence of TrkB clusters in 6-OHDA-treated rats suggests that association of TrkB/SORCS-2 with VPS35 in the retromer complex and thus recycling to the cell surface are impaired. We therefore investigated the association of TrkB/SORCS-2 clusters with VPS35 by co-staining these three proteins in neurons within the DA-depleted hemisphere of hemiparkinsonian rats. As observed before, TrkB and SORCS-2-IR revealed strong signal overlap in perinuclear clusters (Figure S7C). However, we did not observe VPS35-IR in these clusters. This suggests that TrkB/SORCS-2 that is contained within those structures is unavailable for VPS35-mediated membrane re-insertion and recycling and therefore accumulates at these perinuclear sites.

Similar to our *in vitro* observation (Figures 1H and 1I), TrkB clusters appeared closely associated with structures of the lysosomal degradational pathway. To test this hypothesis, we stained TrkB with the lysosomal marker Cathepsin D, which identified dense accumulation at the site of TrkB clusters (Figure 4E). High-resolution SIM microscopy revealed that Cathepsin D-IR did not co-localize with TrkB but rather appears to surround the TrkB clusters (Figure 4F), similar to Lamp-1-positive structures surrounding TrkB clusters in DA-depleted FACS dSPNs (Figures 1H, left, and 1I).

Interaction of SORCS-2 with VPS35 in the retromer complex[40] does not only regulate surface expression of transmembrane proteins[69,70] but also prevents their lysosomal degradation.[39] The observation that TrkB clusters are surrounded by lysosomal vesicles suggests impaired ER-to-lysosome-associated degradation (ERLAD). This process involves translocation of TrkB from the ER to autophagosomes, which later fuse with lysosomes for cargo degradation. To test whether the TrkB transition to lysosomes is impaired in DA-depleted striatum, we performed correlative light-electron microscopy (CLEM) together with SIM of TrkB and Cathepsin D (Figure 4G). Electron microscopy revealed multivesicular-like perinuclear structures that seemed to be closely associated with ER membranes (Figure 4G, asterisks). Those structures contained multiple electron-dense vesicles that were positive for TrkB-IR and surrounded by Cathepsin D-positive structures (Figure 4G). Our observations reveal that TrkB is translocated to multivesicular bodies in the absence of dopaminergic input and fails to enter lysosomal degradation.

TrkB clusters form Proteinase K-resistant aggregates

Failure to enter lysosomal degradation indicates that TrkB clusters could become insoluble solid protein aggregates. To test this hypothesis, brain sections of hemiparkinsonian rats were treated with Proteinase K (PK), using an assay that is commonly used to identify insoluble alpha-synuclein aggregates.[71,72] TH, DARPP-32, and TrkB-IR, using the AF1494 antiserum, were clearly detectable on the intact hemisphere before PK treatment (Figure 5A). TrkB clusters in the DA-depleted hemisphere persisted after PK treatment, whereas DARPP-32-IR was completely erased (Figure 5B). To test whether TrkB is inaccessible to PK due to surrounding membranes in a multivesicular body-like compartment, we compared TrkB-IR with the Golgi matrix protein GM130 (Figure 5C). Again, cytosolic DARPP-32 and Golgi-associated GM130 were completely digested by PK, whereas TrkB-IR persisted in clusters (Figure 5C). To exclude the possibility that the AF1494 antibody detects non-digested

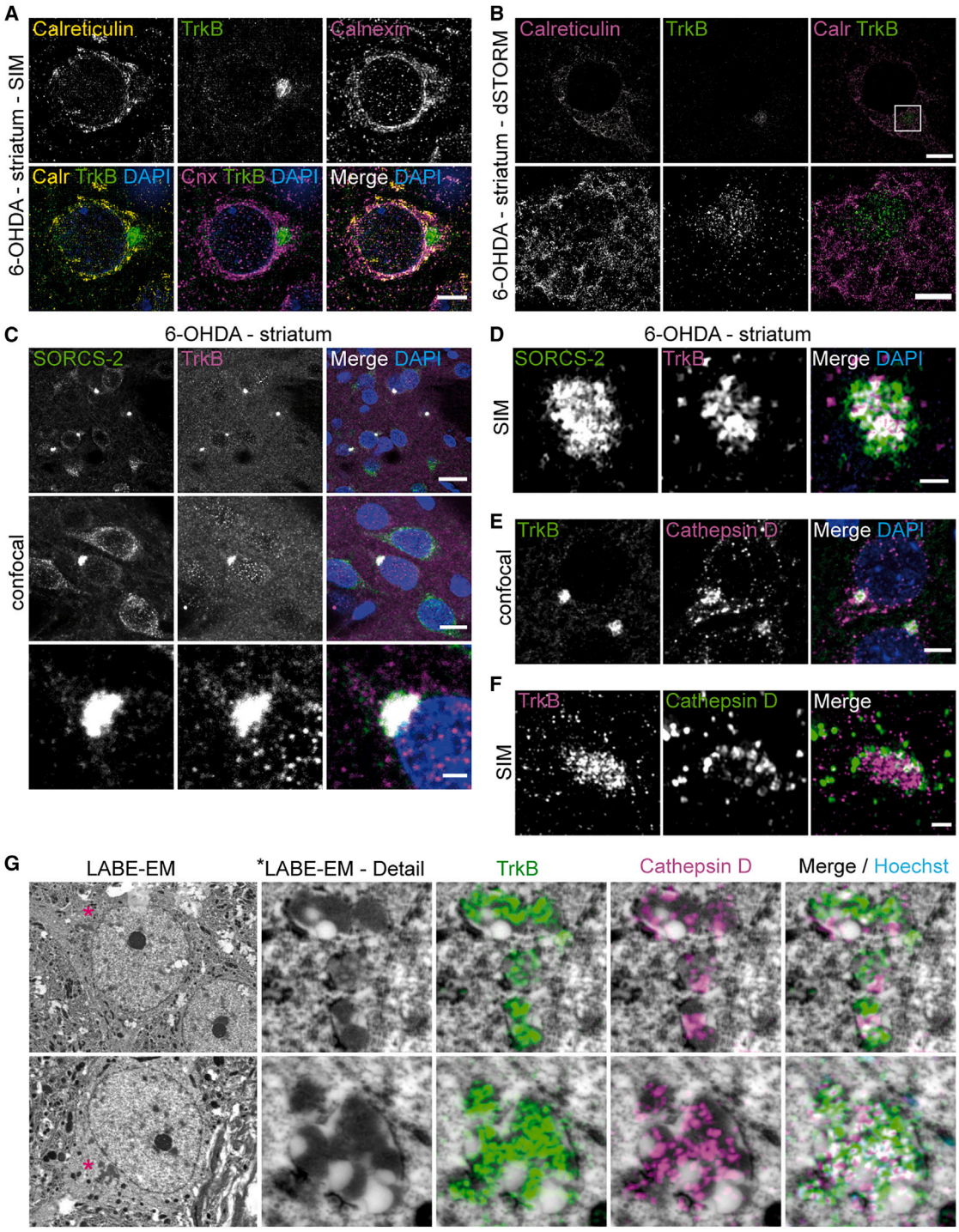

Figure 4. TrkB clusters co-localize with cargo receptor SORCS-2, required for cell-surface expression, and fail to fuse with lysosomal compartments for degradation

(A) High-resolution SIM-IHC image of a dSPN in dopamine-depleted rat striatum, with TrkB cluster occurring in regional proximity to the ER markers Calreticulin and Calnexin, without showing signal overlap.

(B) Super-resolution dSTORM image of a TrkB cluster together with the luminal ER protein Calreticulin in a dSPN of dopamine-depleted dorsolateral rat striatum.

(C) Confocal IHC reveals signal overlap between TrkB-IR and SORCS2-IR. These molecules colocalize to the same cluster-like structures in dSPNs. Note that SORCS2-IR is mislocalized in dSPNs containing a TrkB cluster, compared with neighboring SPNs without such a TrkB cluster.

(D) High-resolution SIM-IHC image showing signal overlap between TrkB- and SORCS2-IR in perinuclear TrkB cluster.

(legend continued on next page)

TrkB extracellular fragments that are protected against PK digestion by hyperglycosylation, we tested a Pan-Trk antibody (EPR17341) against the receptor C terminus. The specificity of this antibody was confirmed by colocalization with another validated pan-Trk antibody (C17F3) in brain sections from hemiparkinsonian rats (Figures S8A–S8D). Pan-Trk (EPR17341) also revealed signal overlap with the AF1494 antiserum (Figures S8C and S8D) and SORCS-2 (Figure S8E). To exclude that these antibodies detect clustered truncated TrkB, we also used a specific antibody against truncated TrkB-T1, which failed to identify any clusters (Figure S8F).

Similar as observed with the TrkB antiserum AF1494, Pan-Trk-IR-positive perinuclear clusters could not be degraded by PK treatment (Figure 5D). Interestingly, we also observed Pan-Trk staining in ER-like structures in addition to these clusters before PK treatment. This staining was mostly lost after PK digestion (Figure 5E). Finally, we tested whether activated TrkB is present within the cluster and stained against pTrk-PLC-y. No obvious pTrk signal was observed at the sites of TrkB clusters at high magnification (Figure 5F), suggesting that TrkB clusters did not contain previously activated TrkB receptors.

Total TrkB protein levels increase in DA-depleted striatum

TrkB aggregation could be a consequence of abnormal receptor degradation, leading to increased TrkB protein levels. To test this hypothesis, we performed WB analyses comparing TrkB protein levels in intact versus DA-depleted striatum extracts after unilateral 6-OHDA injection in adult rats. TrkB full-length protein levels were significantly increased in the DA-depleted striatal hemisphere compared with the control hemisphere (Figures 6A and 6B), when calreticulin protein levels were used as a reference. Because calreticulin levels also could change after 6-OHDA treatment, we additionally normalized TrkB levels to the pan-neuronal marker Tuj1. Similarly, we observed a significant increase in TrkB levels (Figures 6C and 6D). To exclude the possibility that increased TrkB protein levels in the DA-depleted striatum are a consequence of elevated gene expression, we performed qRT-PCR analyses of TrkB mRNA levels. TrkB mRNA levels were not altered in DA-depleted striatum, suggesting that increased protein levels are indeed the result of impaired receptor degradation (Figure 6E). Furthermore, we observed a significant increase in Cathepsin D protein levels at 1 month, but not 4 months, after 6-OHDA lesion (Figure 6F). At the same time, DARPP-32 levels were found to be significantly upregulated at 1 month after lesion (Figure 6G), whereas they were significantly decreased in DA-depleted striatum at 4 months after lesion (Figure 6G).

Trk cluster formation in postmortem striatal SPNs of patients with PD

We next investigated TrkB cluster formation in striatal SPNs in the postmortem striatum of five patients with PD and five age-matched individuals who died of non-neurological conditions. These postmortem brain sections were stained with the monoclonal pan-Trk antibody (EPR17341).

We observed Pan-Trk-IR throughout the cell body of striatal neurons (Figure 7A). In contrast, PD brain sections revealed Trk-IR in large perinuclear clusters (arrows in Figure 7A). The number of Pan-Trk clusters per square millimeter is significantly increased in postmortem PD striatum compared with controls (Figure 7B). Quantification of the ratio between the diameter of the pan-Trk clusters and the nucleus within the same cell revealed an average ratio of 0.84 (Figure 7C). This ratio in PD postmortem striatal neurons is higher than that observed in 6-OHDA-treated rats (2 weeks: 0.15; 4 weeks: 0.28; 16 weeks: 0.27; Figure 2F). This difference could either be caused by species differences or by the progressed disease state in patients with PD. To ensure that these clusters occur in striatal SPNs, we double-stained Pan-Trk (EPR17341) with the SPN marker DARPP-32. Pan-Trk-IR was observed in DARPP-32-positive striatal SPNs both in control and in patient brain sections. However, Trk-positive clusters were found only in SPNs of patients with PD (Figure 7D, arrows). We next tested whether pan-Trk-IR is part of α-Synuclein-positive Lewy bodies in neuromelanin-positive dopaminergic neurons of the substantia nigra in postmortem PD midbrain (Figure 7E). No significant pan-Trk-IR was observed in Lewy bodies (Figure 7E, upper line). Instead, TrkB-IR was present in small vesicle-like structures and ER-like pattern outside Lewy bodies within the soma of dopaminergic neurons (Figure 7E, black arrows).

The presence of TrkB clusters in the postmortem striatum of patients with PD confirms our observations in hemiparkinsonian rat striatum and FACS SPN cultures. Taken together, these findings indicate that DRD1 positively regulates TrkB surface expression in dSPNs and thus controls the sensitivity of these neurons for cortico-striatal BDNF. In the absence of DRD1 activation, TrkB translocation to postsynaptic sites is prevented. Instead, TrkB accumulates in perinuclear clusters that appear unable to enter normal degradational pathways and undergo a transition into insoluble protein aggregates over time.

DISCUSSION

In this study, we have investigated the modulatory function of striatal DA on SPN sensitivity for BDNF. We found that TrkB

(E) Confocal IHC image showing TrkB and Cathepsin D cluster formation.
(F) High-resolution SIM-IHC image of a TrkB cluster reveals Cathepsin D-positive lysosomal structures surrounding the TrkB cluster.
(G) CLEM of PFA-fixed 40-μm free-floating vibratome sections of 6-OHDA rats at 4 months post-lesion showing correlation of high-resolution SIM-IHC of TrkB clusters with electron microscopic images of dSPNs within DA-depleted rat striatum. Cluster-like structures are evident with electron microscopy (asterisks). High magnification of these clusters reveals multiple vesicle-like structures with high electron density. These multivesicular clusters are in close proximity to the nucleus and ER membranes. TrkB-IR is evident in electron-dense structures surrounded by smaller Cathepsin D-positive vesicles.
Scale bars: 5 μm (A; B, top; and E); 2 μm (B, bottom; C, bottom); 20 μm (C, top); 10 μm (C, middle); 1 μm (D and F).
See also Figure S7.

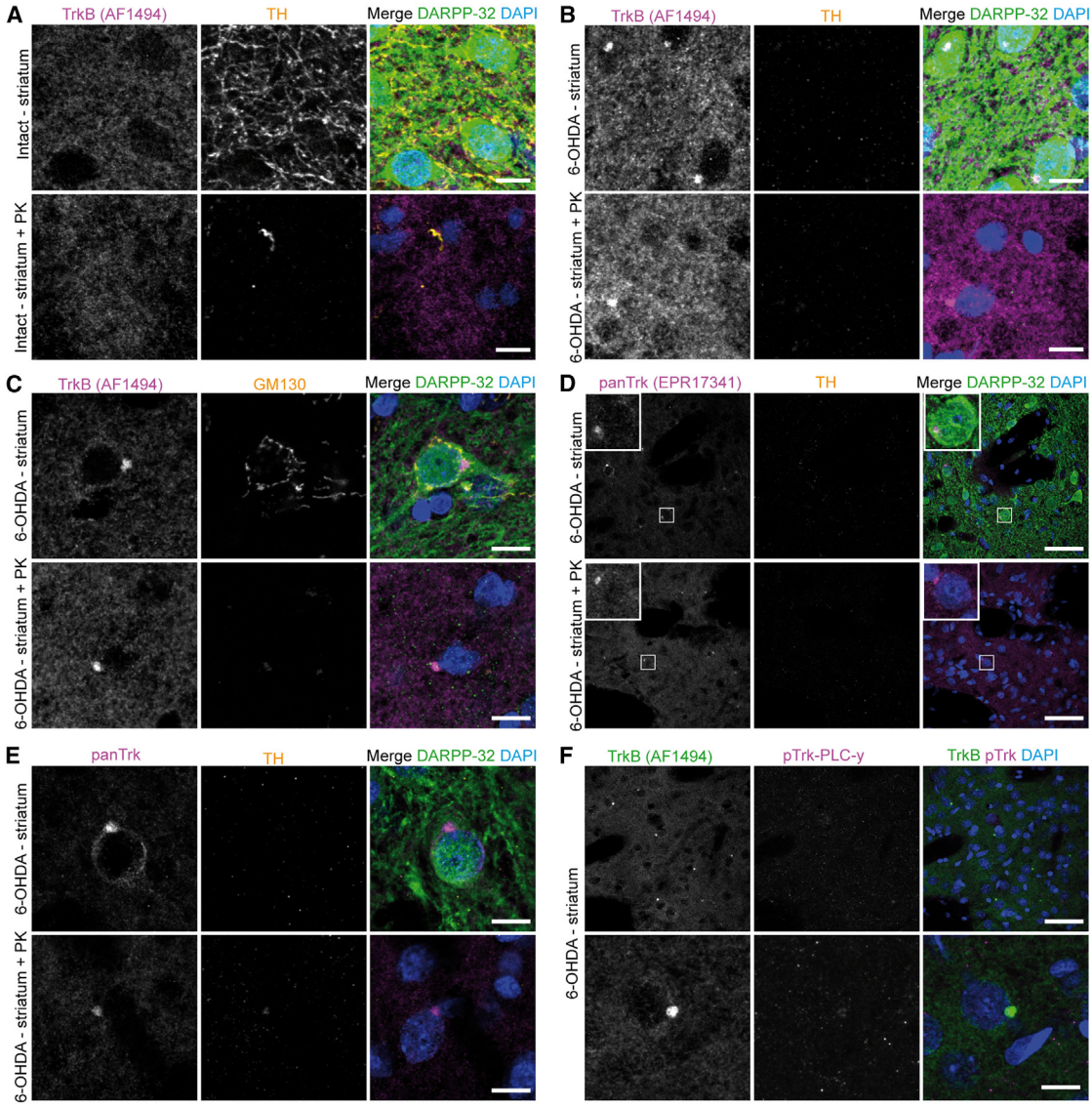

Figure 5. TrkB clusters show properties of Proteinase K-resistant aggregates

(A) Confocal IHC image showing intact dorsolateral striatum before (top) and after Proteinase K treatment (bottom) indicated by complete digestion of DARPP-32 and TH.

(B) Confocal IHC image showing corresponding DA-depleted 6-OHDA dorsolateral striatum of brain sections in A) before (top) and after Proteinase K treatment (bottom). DARPP-32 IHC is lost due to Proteinase K treatment. TrkB was stained using the AF1494 antibody against the extracellular domain. TrkB clusters are still evident after PK digestion.

(C) High-magnification image of TrkB clusters together with Golgi matrix protein GM130 and cytosolic protein DARPP-32 before (top) and after PK treatment. GM130 and DARPP-32-IR are lost after PK digestion, whereas TrkB-IR is still evident.

(D) Confocal IHC image showing DARPP-32, TH, and Trk-IR before (top) and after PK treatment (bottom), using the Pan-Trk (EPR17341) antibody against C-terminal TrkA, B, and C. DARPP-32-IR is completely lost after PK digestion, whereas Trk-IR-positive clusters are still evident.

(E) High-magnification image of Pan-Trk clusters before (top) and after PK treatment. Pan-Trk-IR reveals perinuclear clusters and ER-like signal (top). This ER-like signal is lost by PK treatment, whereas perinuclear clusters are still evident (bottom).

(F) Confocal IHC image of TrkB (AF1494) and pTrk-PLC-y. High-magnification image reveals that pTrk-PLC-y-IR is absent from TrkB clusters.

Scale bars: 50 μm (D, and F, top); 10 μm (A–C, E, and F, bottom). See also Figure S8.

cell-surface expression depends on GPCR signaling through DRD1, resulting in elevated sensitivity for BDNF in dSPNs. Absence of DRD1 activation in dSPNs causes the formation of perinuclear TrkB clusters. Such clusters are detectable both *in vitro* and *in vivo*, as well as in the basal ganglia of postmortem brains of patients with PD. These TrkB clusters are associated with SORCS-2, a cargo receptor required for TrkB transport to dendritic membranes and potentiated PSDs.[38] TrkB degradation through the lysosomal machinery appears impaired, allowing the formation of PK-resistant insoluble TrkB aggregates.

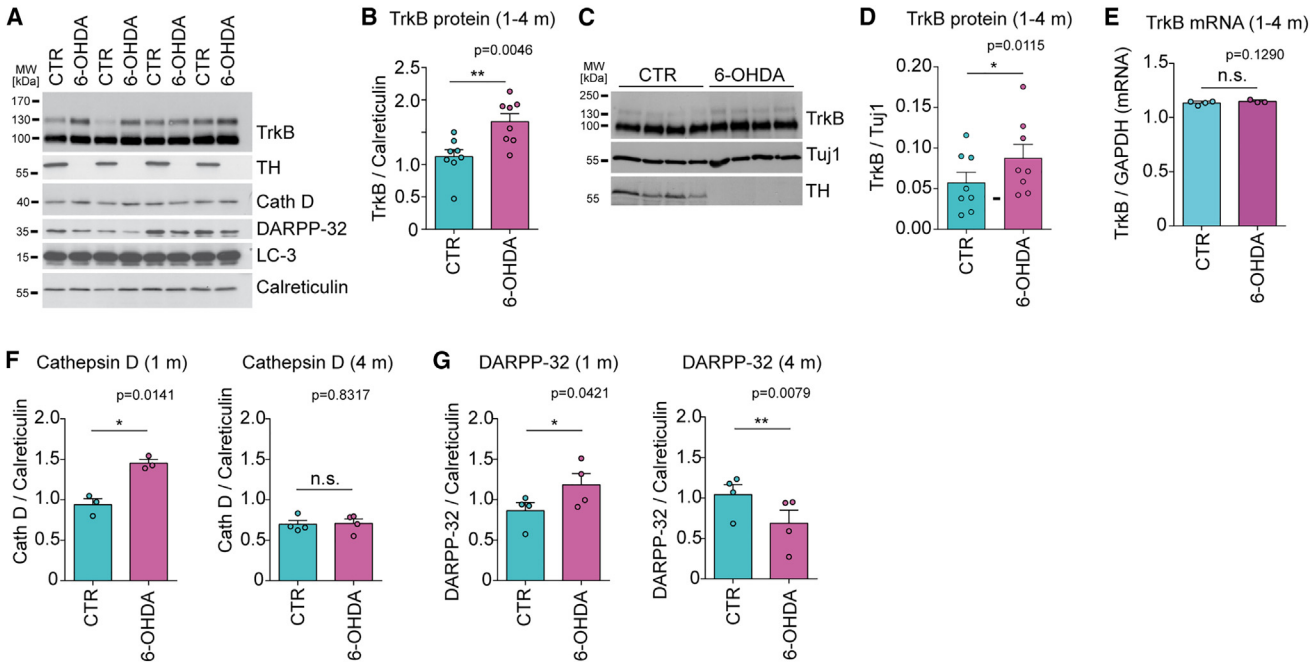

Figure 6. Total TrkB levels are altered in dopamine-depleted striatum

(A) WB of 6-OHDA rat striatum at 4 months after lesion.

(B) Quantification of TrkB protein levels in adult rats reveals a significant increase in total TrkB (n = 8/condition; p = 0.0046, paired t test) in DA-depleted striatum with calreticulin as a reference standard.

(C) Reanalysis of the samples shown in (A). WB of 6-OHDA rat striatum at 4 months after lesion probed for TrkB, Tuj1, and TH.

(D) Quantification of TrkB protein levels normalized to Tuj1 confirms a significant increase in total TrkB (n = 8/condition; p = 0.0115, paired t test) in DA-depleted striatum.

(E) qRT-PCR analysis for TrkB-FL mRNA comparing intact versus dopamine-depleted striatum in adult rats after 6-OHDA lesion reveals no effect of 6-OHDA lesion on TrkB transcription (n = 4 for control, n = 3 for 6-OHDA; paired t test).

(F) Total Cathepsin D levels are increased at 1 month after lesion (n = 3/condition for 1 month and n = 4/condition for 4 months; p = 0.0141, paired t test) and appear unchanged at 4 months after lesion.

(G) DARPP-32 levels are significantly increased in DA-depleted striatum at 1 month (p = 0.0421, paired t test) and decreased at 4 months after lesion (n = 4/condition; p = 0.0079).

Data are shown as mean ± SEM; paired t test, $^{n.s.}p > 0.05$; $^{*}p \leq 0.05$; $^{**}p \leq 0.01$; $^{***}p \leq 0.001$; $^{****}p \leq 0.0001$.

BDNF/TrkB signaling is an essential regulator of cortico-striatal synaptic plasticity.[6,27,28] LTP at these synapses occurs mainly postsynaptically in striatal SPNs and involves activation of TrkB.[5,6,28] Its function differs from the well-characterized hippocampal LTP induction at CA1 Schaffer collaterals, where TrkB is involved both pre- and postsynaptically.[73–75] In addition, lack of BDNF causes more dramatic effects on morphology and plasticity of postsynaptic neurons at cortico-striatal compared with intrahippocampal synapses.[27,76,77] In both regions, synaptic plasticity depends on NMDAR and α-amino-3-hydroxy-5-methyl-4-isoxazolepropionic acid (AMPA)-R-mediated responses.[73,74,78,79] As an important difference, cortico-striatal synaptic plasticity does not only involve activation of postsynaptic NMDAR and TrkB but requires additional GPCR signaling through DA receptors.[5,6,24] A direct link between striatal DRD1 and TrkB signaling is suggested by several observations. First, TrkB is expressed together with DRD1 in dSPNs.[4,6] Second, loss of either presynaptic BDNF or inhibition of postsynaptic TrkB abolishes LTP in SPNs.[6,27] Similarly, striatal DA depletion abolishes striatal synaptic plasticity,[5,16,80] as does depletion of the downstream effector DARPP-32 in striatal SPNs.[81] Third, cAMP is required for TrkB cell-surface expression and sensitivity to BDNF,[37] and DA receptors modulate cAMP levels via control of adenylyl-cyclase activity.[21] DRD1 increases cAMP via $G_{\alpha s/olf}$-mediated AC stimulation.[21,82–87] This suggests that DA acting through DRD1 in dSPNs increases cAMP and alters TrkB cell-surface expression, thereby modulating sensitivity for BDNF in the context of cortico-striatal synaptic plasticity. However, presynaptic TrkB activation might also occur and contribute to cortico-striatal plasticity. Optogenetic stimulation of M1 cortical axons has been shown to result in BDNF-dependent LTP both at pre- and postsynaptic sites at cortico-striatal synapses.[28] Interestingly, presynaptic plasticity and spontaneous activity of iSPNs appear normal in mice lacking TrkB in enkephalin-positive striatopallidal iSPNs,[88] although these mice show hyperlocomotion. Thus, postsynaptic TrkB appears essential for integration of cortical glutamatergic input into these circuits.[88]

Our observation that DRD1 $G_{\alpha s/olf}$ activation increases sensitivity to BDNF in dSPNs points to a mode of modulation of cortico-striatal synaptic plasticity through promoting postsynaptic LTP in dSPNs.[4,5,24,26] This function is antagonized by M4R-$G_{\alpha i}$.[4,5,16,24,89]

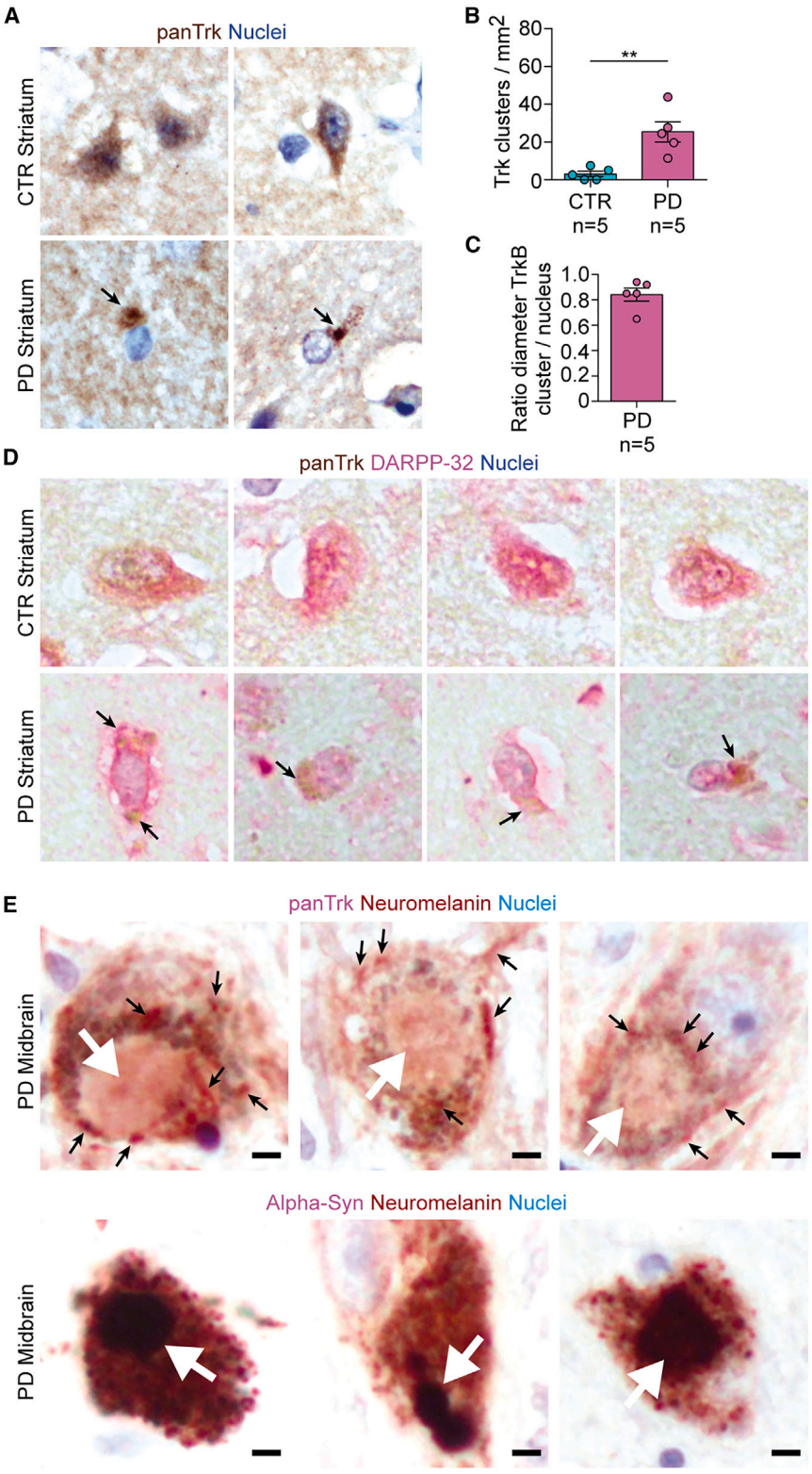

Figure 7. Trk receptor cluster formation in striatal SPNs of patients with PD

(A) Representative Pan-Trk 3,3′-Diaminobenzidin (DAB)-IHC staining in postmortem corpus striatum derived from two controls (top) and two patients with PD (bottom). Pan-Trk cluster formation is evident in PD patient corpus striatum (black arrows).

(B) Quantification of Trk receptor cluster formation per mm^2 in n = 5 controls versus n = 5 patients with PD reveals significant increase in Trk receptor cluster formation in patients with PD. Data are shown as mean ± SEM; Student's t test, p = 0.0038; p > 0.05; *p ≤ 0.05; **p ≤ 0.01; ***p ≤ 0.001; ****p ≤ 0.0001.

(C) Quantification of the ratio between Trk cluster and nuclear diameters in n = 5 patients. Data are shown as mean ± SEM.

(D) Co-staining of Pan-Trk (DAB) and DARPP-32 (alkaline phosphatase, AP) reveals Pan-Trk-cluster (black arrows) formation in DARPP-32-positive striatal SPNs in patients with PD.

(E) Pan-Trk-IR (AP) in neuromelanin (brown) containing midbrain dopaminergic neurons (black arrows, top) that contain an α-Synuclein aggregate (white arrows). PanTrk-IR is evident in small vesicle-like structures and ER-like patterns, outside Lewy bodies. α-Synuclein aggregates (AP) were labeled in a separate staining (white arrows, lower panels). α-Synuclein aggregates do not stain for pan-Trk-IR. Scale bars: 10 μm.

DRD1 activation apparently does not only promote TrkB translocation toward the cell surface but also leads to increased TrkB/SORCS-2 co-localization in peripheral neurites. A specific role of SORCS-2 in BDNF-dependent long-term synaptic plasticity has recently been shown in hippocampal neurons.[38] This mechanism is functionally important for memory formation, indicating that it plays a central role in BDNF/TrkB-mediated synaptic plasticity processes in the hippocampus. This is similar in DA-depleted dSPNs that also show reduced TrkB cell-surface expression and BDNF sensitivity. Instead, DA-depleted dSPNs reveal perinuclear clusters of TrkB together with SORCS-2. The observation that SORCS-2 is mislocalized to perinuclear clusters in dSPNs when DRD1 signaling is reduced indicates that striatal dopaminergic signaling modulates the distribution of this sorting molecule, and that defects of dopaminergic input can cause accumulation of SORCS-2 in perinuclear ER-like structures. Thus, all cargoes for SORCS-2 might be affected, and the sensitivity for signaling inputs other than BDNF/TrkB might also be reduced by this mechanism. SORCS-2 also prevents the transition of proteins to lysosomal structures,[40] and our results that fusion of multivesicular bodies with lysosomes is highly reduced in the absence of DRD1 activity are in agreement with these observations. Therefore, the degradation of TrkB/SORCS-2 clusters by fusion with lysosomes seems to be controlled by dopaminergic input.

The TrkB aggregates in hemiparkinsonian rat brains are located within multivesicular bodies, suggesting that both TrkB from the ER and endocytosed TrkB from the cell surface accumulate in such structures. The physiological translocation of TrkB from ER to the cell surface could occur either directly[90] or via the TGN. Alternatively, TrkB could transit from endosomes or ER to lysosomes for degradation. Accordingly, TrkB aggregates do not show colocalization with ER (Calreticulin, Calnexin), *cis*-Golgi markers (GM130), or TGMs (TGN-38). Our *in vitro* data with bafilomycin that blocks lysosomal degradation show a massive increase in TrkB/SORCS-2 cluster size, indicating that a substantial amount of TrkB is usually degraded via the lysosomal machinery under conditions even when DRD1 receptors are not activated. Thus, TrkB association with SORCS-2 might not only be dedicated for export to the cell surface but at the same time appears to provide protection from lysosomal degradation. The apparent protective effect of SORCS-2 against lysosomal degradation then causes TrkB accumulation. Finally, such TrkB clusters develop further into insoluble protein aggregates over time that are resistant to PK treatment.

Taken together, our data indicate that DRD1 $G_{\alpha s/olf}$ signaling in dSPNs increases TrkB/SORCS-2 translocation to the cell surface and to peripheral neurites where postsynaptic sites normally are located. This results in increased sensitivity for BDNF. When DRD1 is not activated, either *in vitro* or *in vivo*, perinuclear clusters of TrkB and SORCS-2 form that reflect impaired TrkB translocation to lysosomes. Intracellular retention of TrkB results in decreased sensitivity of dSPNs for BDNF, which is likely to contribute to alterations in synaptic plasticity in DA-depleted dSPN spines.[5,24] This extends previous models of GPCR function in striatal synaptic plasticity by demonstrating the role of GPCR signaling through $G_{\alpha s/olf}$ for TrkB turnover and surface expression, thus modulating BDNF sensitivity. DRD1 and M4R[24] seem to be responsible for such GPCR-mediated effects in dSPNs. It would be important to determine the threshold of striatal DA, which marks the first TrkB cluster formation as an important hallmark of PD progression. Furthermore, it remains to be tested to which extent acute anti-parkinsonian treatment in either 6-OHDA rats or human patients with PD affects TrkB cell-surface expression.

Limitations of the study

The present study mainly uses immunocytochemistry and immunohistochemistry and is thus limited by several factors. The observation of TrkB and SORCS-2-IR in perinuclear clusters and spatial proximity does not allow a conclusion on molecular interaction. Even though TrkB antibodies were extensively tested with TrkB-deficient mouse brain tissues, we cannot exclude that antibodies against TrkB may produce nonspecific binding in rat tissue that may cause background noise, especially seen in PK digestion experiments. Controls showing that DARPP-32, GM130, and TH-IR are digested, but not TrkB-IR, in perinuclear aggregates does not exclude the possibility that at least part of the staining represents background after PK treatment. The finding that TrkB aggregates appear resistant to PK treatment does not allow a conclusion about the composition of the aggregate itself. Therefore, it remains speculative whether other transmembrane receptors are also mislocalized to these aggregates. Our study is mainly based on *in vitro* experiments with enriched dSPN cultures that allow specific stimulation and analyses for DRD1-mediated downstream effects but lack network activity and physiological synaptic and cellular interactions, for example, with interneurons and thalamic afferents. Other GPCRs might be involved in translocation of TrkB within SPNs[4,5] by creating a balanced activity between $G_{\alpha s/olf}$ and $G_{\alpha i}$. Changes in GPCR activity might shift this balance either toward increased or decreased TrkB cell-surface transport and could thus promote LTP or LTD. Complex neuronal networks including interneurons and astrocytes are required to model such physiological conditions. Finally, we cannot exclude additional effects by BDNF from dopaminergic afferents on striatal SPNs. However, BDNF release from striatal neurons or interneurons can be excluded, because BDNF mRNA is barely present in the striatum.[41]

STAR★METHODS

Detailed methods are provided in the online version of this paper and include the following:

- KEY RESOURCES TABLE
- RESOURCE AVAILABILITY
  - Lead contact
  - Materials availability
  - Data and code availability
- EXPERIMENTAL MODEL AND SUBJECT DETAILS
  - Animals
  - Hemiparkinsonian 6-OHDA lesion
- METHOD DETAILS
  - Cell culture
  - Stimulation of striatal SPNs

- Immunocytochemistry
- Cylinder test
- Preparation of tissue for immunostaining
- Immunohistochemistry – Rat and mouse
- Proteinase K treatment of 6-OHDA rat brain sections
- Immunohistochemistry – Human postmortem tissue
- Correlative light and electron microscopy (CLEM)
- Microscopy
- Western blot analyses
- RNA purification from tissue and RT-PCR

● QUANTIFICATION AND STATISTICAL ANALYSIS

SUPPLEMENTAL INFORMATION

Supplemental information can be found online at https://doi.org/10.1016/j.celrep.2023.112575.

ACKNOWLEDGMENTS

This work was supported by the Deutsche Forschungsgemeinschaft (DFG, German Research Foundation) project 424778381 (TRR 295, A05, A06, and A01), project SE 697/7-1, and project 218894895 (INST 93/761-1 FUGG). R.L.M. was supported by the Alexander von Humboldt-Stiftung. V.P. and C.S. were supported by GRK2581 (P6) SPHINGOINF of the DFG. Work in the lab of R.M. was supported by grant PID2019-111693RB-100 from MICIN/AEI/10.13039/501100011033, the European Union's Horizon 2020 research and innovation program, AND-PD (grant 84800), NextGenerationEU/PRTR (MICIN/CSIC/PTI+ NeuroAging), and CIBERNED, Instituto de Salud Carlos III. The graphical abstract was created with BioRender.com. We thank Drs. James Surmeier, Moses Chao, and Esther Asan for critical comments and suggestions.

AUTHOR CONTRIBUTIONS

T.A., P.L., and M. Sendtner designed research; T.A., P.L., M.R., C.S., D.W., R.L.M., M.A.-O., V.P., R.B., and S.A. performed research; N.G., R.M., and C.M. contributed essential research materials; T.A., P.L., C.W.I., J.V., M. Sauer, and M. Sendtner analyzed data; T.A., P.L., and M. Sendtner edited the paper; T.A. and M. Sendtner wrote the paper.

DECLARATION OF INTERESTS

The authors declare no competing interests.

Received: May 12, 2022
Revised: March 9, 2023
Accepted: May 14, 2023
Published: May 29, 2023

REFERENCES

1. Kawai, R., Markman, T., Poddar, R., Ko, R., Fantana, A.L., Dhawale, A.K., Kampff, A.R., and Ölveczky, B.P. (2015). Motor cortex is required for learning but not for executing a motor skill. Neuron *86*, 800–812. https://doi.org/10.1016/j.neuron.2015.03.024.
2. West, M.O., Carelli, R.M., Pomerantz, M., Cohen, S.M., Gardner, J.P., Chapin, J.K., and Woodward, D.J. (1990). A region in the dorsolateral striatum of the rat exhibiting single-unit correlations with specific locomotor limb movements. J. Neurophysiol. *64*, 1233–1246. https://doi.org/10.1152/jn.1990.64.4.1233.
3. Andreska, T., Rauskolb, S., Schukraft, N., Lüningschrör, P., Sasi, M., Signoret-Genest, J., Behringer, M., Blum, R., Sauer, M., Tovote, P., and Sendtner, M. (2020). Induction of BDNF expression in layer II/III and layer V neurons of the motor cortex is essential for motor learning. J. Neurosci. *40*, 6289–6308. https://doi.org/10.1523/JNEUROSCI.0288-20.2020.
4. Zhai, S., Shen, W., Graves, S.M., and Surmeier, D.J. (2019). Dopaminergic modulation of striatal function and Parkinson's disease. J. Neural. Transm. *126*, 411–422. https://doi.org/10.1007/s00702-019-01997-y.
5. Shen, W., Flajolet, M., Greengard, P., and Surmeier, D.J. (2008). Dichotomous dopaminergic control of striatal synaptic plasticity. Science *321*, 848–851. https://doi.org/10.1126/science.1160575.
6. Plotkin, J.L., Day, M., Peterson, J.D., Xie, Z., Kress, G.J., Rafalovich, I., Kondapalli, J., Gertler, T.S., Flajolet, M., Greengard, P., et al. (2014). Impaired TrkB receptor signaling underlies corticostriatal dysfunction in Huntington's disease. Neuron *83*, 178–188. https://doi.org/10.1016/j.neuron.2014.05.032.
7. Yin, H.H., and Knowlton, B.J. (2006). The role of the basal ganglia in habit formation. Nat. Rev. Neurosci. *7*, 464–476. https://doi.org/10.1038/nrn1919.
8. Lerner, T.N., and Kreitzer, A.C. (2011). Neuromodulatory control of striatal plasticity and behavior. Curr. Opin. Neurobiol. *21*, 322–327. https://doi.org/10.1016/j.conb.2011.01.005.
9. Wickens, J.R., Reynolds, J.N.J., and Hyland, B.I. (2003). Neural mechanisms of reward-related motor learning. Curr. Opin. Neurobiol. *13*, 685–690. https://doi.org/10.1016/j.conb.2003.10.013.
10. Gerfen, C.R., and Surmeier, D.J. (2011). Modulation of striatal projection systems by dopamine. Annu. Rev. Neurosci. *34*, 441–466. https://doi.org/10.1146/annurev-neuro-061010-113641.
11. Kreitzer, A.C., and Malenka, R.C. (2008). Striatal plasticity and basal ganglia circuit function. Neuron *60*, 543–554. https://doi.org/10.1016/j.neuron.2008.11.005.
12. Day, M., Wang, Z., Ding, J., An, X., Ingham, C.A., Shering, A.F., Wokosin, D., Ilijic, E., Sun, Z., Sampson, A.R., et al. (2006). Selective elimination of glutamatergic synapses on striatopallidal neurons in Parkinson disease models. Nat. Neurosci. *9*, 251–259. https://doi.org/10.1038/nn1632.
13. Suárez, L.M., Solís, O., Caramés, J.M., Taravini, I.R., Solís, J.M., Murer, M.G., and Moratalla, R. (2014). L-DOPA treatment selectively restores spine density in dopamine receptor D2–expressing projection neurons in dyskinetic mice. Biol. Psychiatry *75*, 711–722. https://doi.org/10.1016/j.biopsych.2013.05.006.
14. Suarez, L.M., Solis, O., Aguado, C., Lujan, R., and Moratalla, R. (2016). L-DOPA oppositely regulates synaptic strength and spine morphology in D1 and D2 striatal projection neurons in dyskinesia. Cereb. Cortex *26*, 4253–4264. https://doi.org/10.1093/cercor/bhw263.
15. Suarez, L.M., Alberquilla, S., García-Montes, J.R., and Moratalla, R. (2018). Differential synaptic remodeling by dopamine in direct and indirect striatal projection neurons in Pitx3 (−/−) mice, a genetic model of Parkinson's disease. J. Neurosci. *38*, 3619–3630. https://doi.org/10.1523/jneurosci.3184-17.2018.
16. Calabresi, P., Picconi, B., Tozzi, A., and Di Filippo, M. (2007). Dopamine-mediated regulation of corticostriatal synaptic plasticity. Trends Neurosci. *30*, 211–219. https://doi.org/10.1016/j.tins.2007.03.001.
17. Kreitzer, A.C., and Malenka, R.C. (2005). Dopamine modulation of state-dependent endocannabinoid release and long-term depression in the striatum. J. Neurosci. *25*, 10537–10545. https://doi.org/10.1523/JNEUROSCI.2959-05.2005.
18. Lovinger, D.M. (2010). Neurotransmitter roles in synaptic modulation, plasticity and learning in the dorsal striatum. Neuropharmacology *58*, 951–961. https://doi.org/10.1016/j.neuropharm.2010.01.008.
19. Albin, R.L., Young, A.B., and Penney, J.B. (1989). The functional anatomy of basal ganglia disorders. Trends Neurosci. *12*, 366–375. https://doi.org/10.1016/0166-2236(89)90074-x.
20. Suarez, L.M., Solis, O., Sanz-Magro, A., Alberquilla, S., and Moratalla, R. (2020). Dopamine D1 receptors regulate spines in striatal direct-pathway and indirect-pathway neurons. Mov. Disord. *35*, 1810–1821. https://doi.org/10.1002/mds.28174.

21. Tritsch, N.X., and Sabatini, B.L. (2012). Dopaminergic modulation of synaptic transmission in cortex and striatum. Neuron *76*, 33–50. https://doi.org/10.1016/j.neuron.2012.09.023.

22. Gardoni, F., and Bellone, C. (2015). Modulation of the glutamatergic transmission by Dopamine: a focus on Parkinson, Huntington and Addiction diseases. Front. Cell. Neurosci. *9*, 25. https://doi.org/10.3389/fncel.2015.00025.

23. Granado, N., Ortiz, O., Suárez, L.M., Martín, E.D., Ceña, V., Solís, J.M., and Moratalla, R. (2008). D1 but not D5 dopamine receptors are critical for LTP, spatial learning, and LTP-induced arc and zif268 expression in the Hippocampus. Cereb. Cortex *18*, 1–12. https://doi.org/10.1093/cercor/bhm026.

24. Shen, W., Plotkin, J.L., Francardo, V., Ko, W.K.D., Xie, Z., Li, Q., Fieblinger, T., Wess, J., Neubig, R.R., Lindsley, C.W., et al. (2015). M4 muscarinic receptor signaling ameliorates striatal plasticity deficits in models of L-DOPA-induced dyskinesia. Neuron *88*, 762–773. https://doi.org/10.1016/j.neuron.2015.10.039.

25. Yano, H., Cai, N.S., Xu, M., Verma, R.K., Rea, W., Hoffman, A.F., Shi, L., Javitch, J.A., Bonci, A., and Ferré, S. (2018). Gs- versus Golf-dependent functional selectivity mediated by the dopamine D1 receptor. Nat. Commun. *9*, 486. https://doi.org/10.1038/s41467-017-02606-w.

26. Plotkin, J.L., and Surmeier, D.J. (2014). Impaired striatal function in Huntington's disease is due to aberrant p75NTR signaling. Rare Dis. *2*, e968482. https://doi.org/10.4161/2167549X.2014.968482.

27. Jia, Y., Gall, C.M., and Lynch, G. (2010). Presynaptic BDNF promotes postsynaptic long-term potentiation in the dorsal striatum. J. Neurosci. *30*, 14440–14445. https://doi.org/10.1523/JNEUROSCI.3310-10.2010.

28. Park, H., Popescu, A., and Poo, M.M. (2014). Essential role of presynaptic NMDA receptors in activity-dependent BDNF secretion and corticostriatal LTP. Neuron *84*, 1009–1022. https://doi.org/10.1016/j.neuron.2014.10.045.

29. Miller, K.M., Patterson, J.R., Kochmanski, J., Kemp, C.J., Stoll, A.C., Onyekpe, C.U., Cole-Strauss, A., Steece-Collier, K., Howe, J.W., Luk, K.C., and Sortwell, C.E. (2021). Striatal afferent BDNF is disrupted by synucleinopathy and partially restored by STN DBS. J. Neurosci. *41*, 2039–2052. https://doi.org/10.1523/JNEUROSCI.1952-20.2020.

30. Mogi, M., Togari, A., Kondo, T., Mizuno, Y., Komure, O., Kuno, S., Ichinose, H., and Nagatsu, T. (1999). Brain-derived growth factor and nerve growth factor concentrations are decreased in the substantia nigra in Parkinson's disease. Neurosci. Lett. *270*, 45–48. https://doi.org/10.1016/s0304-3940(99)00463-2.

31. Baquet, Z.C., Bickford, P.C., and Jones, K.R. (2005). Brain-derived neurotrophic factor is required for the establishment of the proper number of dopaminergic neurons in the substantia nigra pars compacta. J. Neurosci. *25*, 6251–6259. https://doi.org/10.1523/JNEUROSCI.4601-04.2005.

32. Altar, C.A., Cai, N., Bliven, T., Juhasz, M., Conner, J.M., Acheson, A.L., Lindsay, R.M., and Wiegand, S.J. (1997). Anterograde transport of brain-derived neurotrophic factor and its role in the brain. Nature *389*, 856–860. https://doi.org/10.1038/39885.

33. Andreska, T., Rauskolb, S., Schukraft, N., Lüningschrör, P., Sasi, M., Signoret-Genest, J., Behringer, M., Blum, R., Sauer, M., Tovote, P., and Sendtner, M. (2020). Induction of BDNF expression in layer II/III and layer V neurons of the motor cortex is essential for motor learning. J. Neurosci. *40*, 6289–6308. https://doi.org/10.1523/JNEUROSCI.0288-20.2020.

34. Fumagalli, F., Racagni, G., and Riva, M.A. (2006). Shedding light into the role of BDNF in the pharmacotherapy of Parkinson's disease. Pharmacogenomics J. *6*, 95–104. https://doi.org/10.1038/sj.tpj.6500360.

35. Palasz, E., Wysocka, A., Gasiorowska, A., Chalimoniuk, M., Niewiadomski, W., and Niewiadomska, G. (2020). BDNF as a promising therapeutic agent in Parkinson's disease. Int. J. Mol. Sci. *21*, 1170. https://doi.org/10.3390/ijms21031170.

36. Howells, D.W., Porritt, M.J., Wong, J.Y., Batchelor, P.E., Kalnins, R., Hughes, A.J., and Donnan, G.A. (2000). Reduced BDNF mRNA expression in the Parkinson's disease substantia nigra. Exp. Neurol. *166*, 127–135. https://doi.org/10.1006/exnr.2000.7483.

37. Meyer-Franke, A., Wilkinson, G.A., Kruttgen, A., Hu, M., Munro, E., Hanson, M.G., Jr., Reichardt, L.F., and Barres, B.A. (1998). Depolarization and cAMP elevation rapidly recruit TrkB to the plasma membrane of CNS neurons. Neuron *21*, 681–693. https://doi.org/10.1016/s0896-6273(00)80586-3.

38. Glerup, S., Bolcho, U., Mølgaard, S., Bøggild, S., Vaegter, C.B., Smith, A.H., Nieto-Gonzalez, J.L., Ovesen, P.L., Pedersen, L.F., Fjorback, A.N., et al. (2016). SorCS2 is required for BDNF-dependent plasticity in the hippocampus. Mol. Psychiatry *21*, 1740–1751. https://doi.org/10.1038/mp.2016.108.

39. Steinberg, F., Gallon, M., Winfield, M., Thomas, E.C., Bell, A.J., Heesom, K.J., Tavaré, J.M., and Cullen, P.J. (2013). A global analysis of SNX27-retromer assembly and cargo specificity reveals a function in glucose and metal ion transport. Nat. Cell Biol. *15*, 461–471. https://doi.org/10.1038/ncb2721.

40. Ma, Q., Yang, J., Milner, T.A., Vonsattel, J.P.G., Palko, M.E., Tessarollo, L., and Hempstead, B.L. (2017). SorCS2-mediated NR2A trafficking regulates motor deficits in Huntington's disease. JCI Insight *2*, e88995. https://doi.org/10.1172/jci.insight.88995.

41. Conner, J.M., Lauterborn, J.C., Yan, Q., Gall, C.M., and Varon, S. (1997). Distribution of brain-derived neurotrophic factor (BDNF) protein and mRNA in the normal adult rat CNS: evidence for anterograde axonal transport. J. Neurosci. *17*, 2295–2313.

42. Gorski, J.A., Zeiler, S.R., Tamowski, S., and Jones, K.R. (2003). Brain-derived neurotrophic factor is required for the maintenance of cortical dendrites. J. Neurosci. *23*, 6856–6865.

43. Li, Y., Yui, D., Luikart, B.W., McKay, R.M., Li, Y., Rubenstein, J.L., and Parada, L.F. (2012). Conditional ablation of brain-derived neurotrophic factor-TrkB signaling impairs striatal neuron development. Proc. Natl. Acad. Sci. USA *109*, 15491–15496. https://doi.org/10.1073/pnas.1212899109.

44. Shuen, J.A., Chen, M., Gloss, B., and Calakos, N. (2008). Drd1a-tdTomato BAC transgenic mice for simultaneous visualization of medium spiny neurons in the direct and indirect pathways of the basal ganglia. J. Neurosci. *28*, 2681–2685. https://doi.org/10.1523/JNEUROSCI.5492-07.2008.

45. Puehringer, D., Orel, N., Lüningschrör, P., Subramanian, N., Herrmann, T., Chao, M.V., and Sendtner, M. (2013). EGF transactivation of Trk receptors regulates the migration of newborn cortical neurons. Nat. Neurosci. *16*, 407–415. https://doi.org/10.1038/nn.3333.

46. Shen, W., Plotkin, J.L., Francardo, V., Ko, W.K.D., Xie, Z., Li, Q., Fieblinger, T., Wess, J., Neubig, R.R., Lindsley, C.W., et al. (2016). M4 muscarinic receptor signaling ameliorates striatal plasticity deficits in models of L-DOPA-induced dyskinesia. Neuron *90*, 1139. https://doi.org/10.1016/j.neuron.2016.05.017.

47. Lane, R.F., St George-Hyslop, P., Hempstead, B.L., Small, S.A., Strittmatter, S.M., and Gandy, S. (2012). Vps10 family proteins and the retromer complex in aging-related neurodegeneration and diabetes. J. Neurosci. *32*, 14080–14086. https://doi.org/10.1523/JNEUROSCI.3359-12.2012.

48. Vaegter, C.B., Jansen, P., Fjorback, A.W., Glerup, S., Skeldal, S., Kjolby, M., Richner, M., Erdmann, B., Nyengaard, J.R., Tessarollo, L., et al. (2011). Sortilin associates with Trk receptors to enhance anterograde transport and neurotrophin signaling. Nat. Neurosci. *14*, 54–61. https://doi.org/10.1038/nn.2689.

49. Breiderhoff, T., Christiansen, G.B., Pallesen, L.T., Vaegter, C., Nykjaer, A., Holm, M.M., Glerup, S., and Willnow, T.E. (2013). Sortilin-related receptor SORCS3 is a postsynaptic modulator of synaptic depression and fear extinction. PLoS One *8*, e75006. https://doi.org/10.1371/journal.pone.0075006.

50. Savas, J.N., Ribeiro, L.F., Wierda, K.D., Wright, R., DeNardo-Wilke, L.A., Rice, H.C., Chamma, I., Wang, Y.Z., Zemla, R., Lavallée-Adam, M., et al. (2015). The sorting receptor SorCS1 regulates trafficking of neurexin and

AMPA receptors. Neuron *87*, 764–780. https://doi.org/10.1016/j.neuron.2015.08.007.

51. Xiang, J., Yang, H., Zhao, T., Sun, M., Xu, X., Zhou, X.F., Li, S.H., and Li, X.J. (2014). Huntingtin-associated protein 1 regulates postnatal neurogenesis and neurotrophin receptor sorting. J. Clin. Invest. *124*, 85–98. https://doi.org/10.1172/JCI69206.

52. Ni, X., and Morales, C.R. (2006). The lysosomal trafficking of acid sphingomyelinase is mediated by sortilin and mannose 6-phosphate receptor. Traffic *7*, 889–902. https://doi.org/10.1111/j.1600-0854.2006.00429.x.

53. Canuel, M., Korkidakis, A., Konnyu, K., and Morales, C.R. (2008). Sortilin mediates the lysosomal targeting of cathepsins D and H. Biochem. Biophys. Res. Commun. *373*, 292–297. https://doi.org/10.1016/j.bbrc.2008.06.021.

54. Chen, Z.Y., Ieraci, A., Tanowitz, M., and Lee, F.S. (2005). A novel endocytic recycling signal distinguishes biological responses of Trk neurotrophin receptors. Mol. Biol. Cell *16*, 5761–5772. https://doi.org/10.1091/mbc.e05-07-0651.

55. Dehay, B., Martinez-Vicente, M., Caldwell, G.A., Caldwell, K.A., Yue, Z., Cookson, M.R., Klein, C., Vila, M., and Bezard, E. (2013). Lysosomal impairment in Parkinson's disease. Mov. Disord. *28*, 725–732. https://doi.org/10.1002/mds.25462.

56. Gerfen, C.R. (2006). Indirect-pathway neurons lose their spines in Parkinson disease. Nat. Neurosci. *9*, 157–158. https://doi.org/10.1038/nn0206-157.

57. Jonsson, G. (1980). Chemical neurotoxins as denervation tools in neurobiology. Annu. Rev. Neurosci. *3*, 169–187. https://doi.org/10.1146/annurev.ne.03.030180.001125.

58. Schultz, W. (1982). Depletion of dopamine in the striatum as an experimental model of Parkinsonism: direct effects and adaptive mechanisms. Prog. Neurobiol. *18*, 121–166. https://doi.org/10.1016/0301-0082(82)90015-6.

59. Metz, G.A., Tse, A., Ballermann, M., Smith, L.K., and Fouad, K. (2005). The unilateral 6-OHDA rat model of Parkinson's disease revisited: an electromyographic and behavioural analysis. Eur. J. Neurosci. *22*, 735–744. https://doi.org/10.1111/j.1460-9568.2005.04238.x.

60. Yuan, H., Sarre, S., Ebinger, G., and Michotte, Y. (2005). Histological, behavioural and neurochemical evaluation of medial forebrain bundle and striatal 6-OHDA lesions as rat models of Parkinson's disease. J. Neurosci. Methods *144*, 35–45. https://doi.org/10.1016/j.jneumeth.2004.10.004.

61. Gong, S., Zheng, C., Doughty, M.L., Losos, K., Didkovsky, N., Schambra, U.B., Nowak, N.J., Joyner, A., Leblanc, G., Hatten, M.E., and Heintz, N. (2003). A gene expression atlas of the central nervous system based on bacterial artificial chromosomes. Nature *425*, 917–925. https://doi.org/10.1038/nature02033.

62. Levy, R., Vila, M., Herrero, M.T., Faucheux, B., Agid, Y., and Hirsch, E.C. (1995). Striatal expression of substance P and methionin-enkephalin in genes in patients with Parkinson's disease. Neurosci. Lett. *199*, 220–224. https://doi.org/10.1016/0304-3940(95)12011-r.

63. Gerfen, C.R., McGinty, J.F., and Young, W.S., 3rd. (1991). Dopamine differentially regulates dynorphin, substance P, and enkephalin expression in striatal neurons: in situ hybridization histochemical analysis. J. Neurosci. *11*, 1016–1031.

64. Koizumi, H., Morigaki, R., Okita, S., Nagahiro, S., Kaji, R., Nakagawa, M., and Goto, S. (2013). Response of striosomal opioid signaling to dopamine depletion in 6-hydroxydopamine-lesioned rat model of Parkinson's disease: a potential compensatory role. Front. Cell. Neurosci. *7*, 74. https://doi.org/10.3389/fncel.2013.00074.

65. Young, W.S., 3rd, Bonner, T.I., and Brann, M.R. (1986). Mesencephalic dopamine neurons regulate the expression of neuropeptide mRNAs in the rat forebrain. Proc. Natl. Acad. Sci. USA *83*, 9827–9831. https://doi.org/10.1073/pnas.83.24.9827.

66. Xu, M., Moratalla, R., Gold, L.H., Hiroi, N., Koob, G.F., Graybiel, A.M., and Tonegawa, S. (1994). Dopamine D1 receptor mutant mice are deficient in striatal expression of dynorphin and in dopamine-mediated behavioral responses. Cell *79*, 729–742. https://doi.org/10.1016/0092-8674(94)90557-6.

67. Assali, D.R., Sidikpramana, M., Villa, A.P., Falkenstein, J., and Steele, A.D. (2021). Type 1 dopamine receptor (D1R)-independent circadian food anticipatory activity in mice. PLoS One *16*, e0242897. https://doi.org/10.1371/journal.pone.0242897.

68. Drago, J., Gerfen, C.R., Lachowicz, J.E., Steiner, H., Hollon, T.R., Love, P.E., Ooi, G.T., Grinberg, A., Lee, E.J., Huang, S.P., et al. (1994). Altered striatal function in a mutant mouse lacking D1A dopamine receptors. Proc. Natl. Acad. Sci. USA *91*, 12564–12568. https://doi.org/10.1073/pnas.91.26.12564.

69. Bonifacino, J.S., and Hurley, J.H. (2008). Retromer. Curr. Opin. Cell Biol. *20*, 427–436. https://doi.org/10.1016/j.ceb.2008.03.009.

70. Small, S.A., and Petsko, G.A. (2015). Retromer in Alzheimer disease, Parkinson disease and other neurological disorders. Nat. Rev. Neurosci. *16*, 126–132. https://doi.org/10.1038/nrn3896.

71. Henrich, M.T., Geibl, F.F., Lakshminarasimhan, H., Stegmann, A., Giasson, B.I., Mao, X., Dawson, V.L., Dawson, T.M., Oertel, W.H., and Surmeier, D.J. (2020). Determinants of seeding and spreading of alpha-synuclein pathology in the brain. Sci. Adv. *6*, eabc2487. https://doi.org/10.1126/sciadv.abc2487.

72. Henrich, M.T., Geibl, F.F., Lee, B., Chiu, W.H., Koprich, J.B., Brotchie, J.M., Timmermann, L., Decher, N., Matschke, L.A., and Oertel, W.H. (2018). A53T-alpha-synuclein overexpression in murine locus coeruleus induces Parkinson's disease-like pathology in neurons and glia. Acta Neuropathol. Commun. *6*, 39. https://doi.org/10.1186/s40478-018-0541-1.

73. Xu, B., Gottschalk, W., Chow, A., Wilson, R.I., Schnell, E., Zang, K., Wang, D., Nicoll, R.A., Lu, B., and Reichardt, L.F. (2000). The role of brain-derived neurotrophic factor receptors in the mature hippocampus: modulation of long-term potentiation through a presynaptic mechanism involving TrkB. J. Neurosci. *20*, 6888–6897.

74. Kauer, J.A., Malenka, R.C., and Nicoll, R.A. (1988). A persistent postsynaptic modification mediates long-term potentiation in the hippocampus. Neuron *1*, 911–917. https://doi.org/10.1016/0896-6273(88)90148-1.

75. Minichiello, L. (2009). TrkB signalling pathways in LTP and learning. Nat. Rev. Neurosci. *10*, 850–860. https://doi.org/10.1038/nrn2738.

76. Rauskolb, S., Zagrebelsky, M., Dreznjak, A., Deogracias, R., Matsumoto, T., Wiese, S., Erne, B., Sendtner, M., Schaeren-Wiemers, N., Korte, M., and Barde, Y.A. (2010). Global deprivation of brain-derived neurotrophic factor in the CNS reveals an area-specific requirement for dendritic growth. J. Neurosci. *30*, 1739–1749. https://doi.org/10.1523/JNEUROSCI.5100-09.2010.

77. Baydyuk, M., Russell, T., Liao, G.Y., Zang, K., An, J.J., Reichardt, L.F., and Xu, B. (2011). TrkB receptor controls striatal formation by regulating the number of newborn striatal neurons. Proc. Natl. Acad. Sci. USA *108*, 1669–1674. https://doi.org/10.1073/pnas.1004744108.

78. Muller, D., Joly, M., and Lynch, G. (1988). Contributions of quisqualate and NMDA receptors to the induction and expression of LTP. Science *242*, 1694–1697. https://doi.org/10.1126/science.2904701.

79. Muller, D., and Lynch, G. (1988). Long-term potentiation differentially affects two components of synaptic responses in hippocampus. Proc. Natl. Acad. Sci. USA *85*, 9346–9350. https://doi.org/10.1073/pnas.85.23.9346.

80. Kreitzer, A.C., and Malenka, R.C. (2007). Endocannabinoid-mediated rescue of striatal LTD and motor deficits in Parkinson's disease models. Nature *445*, 643–647. https://doi.org/10.1038/nature05506.

81. Calabresi, P., Gubellini, P., Centonze, D., Picconi, B., Bernardi, G., Chergui, K., Svenningsson, P., Fienberg, A.A., and Greengard, P. (2000). Dopamine and cAMP-regulated phosphoprotein 32 kDa controls both striatal

long-term depression and long-term potentiation, opposing forms of synaptic plasticity. J. Neurosci. *20*, 8443–8451.

82. Memo, M., Missale, C., Carruba, M.O., and Spano, P.F. (1986). Pharmacology and biochemistry of dopamine receptors in the central nervous system and peripheral tissue. J. Neural. Transm. Suppl. *22*, 19–32.

83. Dearry, A., Gingrich, J.A., Falardeau, P., Fremeau, R.T., Jr., Bates, M.D., and Caron, M.G. (1990). Molecular cloning and expression of the gene for a human D1 dopamine receptor. Nature *347*, 72–76. https://doi.org/10.1038/347072a0.

84. Monsma, F.J., Jr., Mahan, L.C., McVittie, L.D., Gerfen, C.R., and Sibley, D.R. (1990). Molecular cloning and expression of a D1 dopamine receptor linked to adenylyl cyclase activation. Proc. Natl. Acad. Sci. USA *87*, 6723–6727. https://doi.org/10.1073/pnas.87.17.6723.

85. Zhou, Q.Y., Grandy, D.K., Thambi, L., Kushner, J.A., Van Tol, H.H., Cone, R., Pribnow, D., Salon, J., Bunzow, J.R., and Civelli, O. (1990). Cloning and expression of human and rat D1 dopamine receptors. Nature *347*, 76–80. https://doi.org/10.1038/347076a0.

86. Sugamori, K.S., Demchyshyn, L.L., Chung, M., and Niznik, H.B. (1994). D1A, D1B, and D1C dopamine receptors from Xenopus laevis. Proc. Natl. Acad. Sci. USA *91*, 10536–10540.

87. Demchyshyn, L.L., Sugamori, K.S., Lee, F.J., Hamadanizadeh, S.A., and Niznik, H.B. (1995). The dopamine D1D receptor. Cloning and characterization of three pharmacologically distinct D1-like receptors from Gallus domesticus. J. Biol. Chem. *270*, 4005–4012.

88. Besusso, D., Geibel, M., Kramer, D., Schneider, T., Pendolino, V., Picconi, B., Calabresi, P., Bannerman, D.M., and Minichiello, L. (2013). BDNF-TrkB signaling in striatopallidal neurons controls inhibition of locomotor behavior. Nat. Commun. *4*, 2031. https://doi.org/10.1038/ncomms3031.

89. Reynolds, J.N., Hyland, B.I., and Wickens, J.R. (2001). A cellular mechanism of reward-related learning. Nature *413*, 67–70. https://doi.org/10.1038/35092560.

90. Hanus, C., Geptin, H., Tushev, G., Garg, S., Alvarez-Castelao, B., Sambandan, S., Kochen, L., Hafner, A.S., Langer, J.D., and Schuman, E.M. (2016). Unconventional secretory processing diversifies neuronal ion channel properties. Elife *5*, e20609. https://doi.org/10.7554/eLife.20609.

91. Granado, N., Escobedo, I., O'Shea, E., Colado, I., and Moratalla, R. (2008). Early loss of dopaminergic terminals in striosomes after MDMA administration to mice. Synapse *62*, 80–84. https://doi.org/10.1002/syn.20466.

92. Markert, S.M., Bauer, V., Muenz, T.S., Jones, N.G., Helmprobst, F., Britz, S., Sauer, M., Rössler, W., Engstler, M., and Stigloher, C. (2017). 3D subcellular localization with superresolution array tomography on ultrathin sections of various species. Methods Cell Biol. *140*, 21–47. https://doi.org/10.1016/bs.mcb.2017.03.004.

93. Markert, S.M., Britz, S., Proppert, S., Lang, M., Witvliet, D., Mulcahy, B., Sauer, M., Zhen, M., Bessereau, J.L., and Stigloher, C. (2016). Filling the gap: adding super-resolution to array tomography for correlated ultrastructural and molecular identification of electrical synapses at the C. elegans connectome. Neurophotonics *3*, 041802. https://doi.org/10.1117/1.NPh.3.4.041802.

94. Peters, S., Kaiser, L., Fink, J., Schumacher, F., Perschin, V., Schlegel, J., Sauer, M., Stigloher, C., Kleuser, B., Seibel, J., and Schubert-Unkmeir, A. (2021). Click-correlative light and electron microscopy (click-AT-CLEM) for imaging and tracking azido-functionalized sphingolipids in bacteria. Sci. Rep. *11*, 4300. https://doi.org/10.1038/s41598-021-83813-w.

95. Reynolds, E.S. (1963). The use of lead citrate at high pH as an electron-opaque stain in electron microscopy. J. Cell Biol. *17*, 208–212. https://doi.org/10.1083/jcb.17.1.208.

96. Andreska, T., Aufmkolk, S., Sauer, M., and Blum, R. (2014). High abundance of BDNF within glutamatergic presynapses of cultured hippocampal neurons. Front. Cell. Neurosci. *8*, 107. https://doi.org/10.3389/fncel.2014.00107.

97. van de Linde, S., Löschberger, A., Klein, T., Heidbreder, M., Wolter, S., Heilemann, M., and Sauer, M. (2011). Direct stochastic optical reconstruction microscopy with standard fluorescent probes. Nat. Protoc. *6*, 991–1009. https://doi.org/10.1038/nprot.2011.336.

98. Costes, S.V., Daelemans, D., Cho, E.H., Dobbin, Z., Pavlakis, G., and Lockett, S. (2004). Automatic and quantitative measurement of protein-protein colocalization in live cells. Biophys. J. *86*, 3993–4003. https://doi.org/10.1529/biophysj.103.038422.

99. Chomczynski, P., and Sacchi, N. (1987). Single-step method of RNA isolation by acid guanidinium thiocyanate-phenol-chloroform extraction. Anal. Biochem. *162*, 156–159. https://doi.org/10.1006/abio.1987.9999.

STAR★METHODS

KEY RESOURCES TABLE

REAGENT or RESOURCE	SOURCE	IDENTIFIER
Antibodies		
Rabbit polyclonal anti RFP	Rockland	Cat# 600-401-379; RRID: AB_2209751
Chicken polyclonal anti GFP	Abcam	Cat# ab13970; RRID: AB_300798
Goat polyclonal anti DARPP-32	R and D Systems	Cat# AF6259; RRID: AB_10641854
Rabbit monoclonal anti DARPP-32	Cell Signaling Technology	Cat# 2306; RRID: AB_823479
Rabbit monoclonal anti pTrk kinase domain	Cell Signaling Technology	Cat# 4621; RRID: AB_916186
Rabbit monoclonal anti pTrk PLC-γ	Cell Signaling Technology	Cat# 4168; RRID: AB_10620952
Rabbit polyclonal anti TrkB	Millipore	Cat# 07–225; RRID: AB_310445
Rabbit monoclonal anti Pan-Trk	Cell Signaling Technology	Cat# 4609; RRID: AB_2236264
Rabbit monoclonal anti Pan-Trk	Abcam	Cat# ab181560
Goat polyclonal anti mTrkB	R and D Systems	Cat# AF1494; RRID: AB_2155264
Chicken polyclonal anti Calreticulin	Thermo Fisher Scientific	Cat# PA1-902A; RRID: AB_2069607
Mouse monoclonal anti Pan-Cadherin	Sigma-Aldrich	Cat# C1821; RRID: AB_476826
Rabbit polyclonal anti TH	Millipore	Cat# AB152; RRID: AB_390204
Chicken polyclonal anti TH	Abcam	Cat# ab76442; RRID: AB_1524535
Rabbit polyclonal anti Methionine-Enkephalin	ImmunoStar	Cat# 20065; RRID: AB_572250
Guinea Pig polyclonal anti Substance P	Novus Biologicals	Cat# NB300-87; RRID: AB_2240296
Rabbit monoclonal anti SHP-2	Cell Signaling Technology	Cat# 3397; RRID: AB_2174959
Rat monoclonal anti HA-tag	Roche	Cat#11867431001; RRID: AB_390919
Goat polyclonal anti Calnexin	SICGEN	Cat# AB0037-200; RRID: AB_2333117
Sheep polyclonal antiSORCS-2	R and D Systems	Cat# AF4237; RRID: AB_2192264
Goat polyclonal anti Cathepsin D	Santa Cruz Biotechnology	Cat# sc-6494; RRID: AB_2087097
Mouse monoclonal anti GM130	BD Biosciences	Cat# 610822; RRID: AB_398141
Mouse monoclonal anti TGN-38	Novus Biologicals	Cat# NB300-575; RRID: AB_2240559
Rabbit monoclonal anti LC-3B	Cell Signaling Technology	Cat# 3868; RRID: AB_2137707
Rat monoclonal anti Lamp-1	Developmental Studies Hybridoma Bank	Cat# 1D4B-S; RRID: AB_528127
Rabbit anti VPS-35	Abcam	Cat# ab157220; RRID: AB_2636885
Donkey anti Mouse DyLight549	Jackson Immunoresearch	Cat# 715-505-150
Donkey anti Mouse DyLight550	Thermo Fisher Scientific	#SA5-10167; RRID: AB_2556747
Donkey anti Rabbit Alexa 488	Jackson Immunoresearch	Cat# 711-545-152; RRID: AB_2313584
Donkey anti Rabbit DyLight550	Thermo Fisher Scientific	Cat# SA5-10039; RRID: AB_2556619
Donkey anti Rabbit Cy3	Jackson Immunoresearch	Cat# 711-165-152; RRID: AB_2307443
Donkey anti Goat Cy3	Jackson Immunoresearch	Cat# 705-165-147; RRID: AB_2307351
Donkey anti Rabbit Cy5	Jackson Immunoresearch	Cat# 711-175-152; RRID: AB_2340607
Donkey anti Rabbit Alexa 647	Jackson Immunoresearch	Cat# 711-605-152; RRID: AB_2492288
Donkey anti Rabbit DyLight649	Jackson Immunoresearch	Cat# 711-495-152; RRID: AB_2315775
Donkey anti Goat Cy2	Jackson Immunoresearch	Cat# 705-225-003; RRID: AB_2340420
Donkey anti Goat Alexa 488	Jackson Immunoresearch	Cat# 705-545-147; RRID: AB_2336933
Donkey anti Goat DyLight550	Thermo Fisher Scientific	Cat# SA5-10087; RRID: AB_2556667
Donkey anti Goat Alexa 647	Jackson Immunoresearch	Cat# 705-605-003; RRID: AB_2340436
Donkey anti Chicken Alexa 488	Jackson Immunoresearch	Cat# 703-545-155; RRID: AB_2340375
Donkey anti Chicken Alexa 647	Jackson Immunoresearch	Cat# 703-605-155; RRID: AB_2340379
Goat anti Chicken Alexa 633	Thermo Fisher Scientific	Cat# A-21103; RRID: AB_2535756

(*Continued on next page*)

Continued

REAGENT or RESOURCE	SOURCE	IDENTIFIER
Donkey anti Rat Cy3	Jackson Immunoresearch	Cat# 712-165-150; RRID: AB_2340666
Donkey anti Goat POD	Jackson Immunoresearch	Cat# 705-035-003; RRID: AB_2340390
Donkey anti Rabbit POD	Jackson Immunoresearch	Cat# 711-035-152; RRID: AB_10015282
Rabbit anti Chicken POD	Jackson Immunoresearch	Cat# 303-035-003; RRID: AB_2339290
Donkey anti Chicken POD	Jackson Immunoresearch	Cat# 703-035-155; RRID: AB_10015283
Horse anti Mouse POD	Cell Signaling Technology	Cat# 7076; RRID: AB_330924
Biological samples		
Human postmortem tissue	Institute of Neuropathology University Hospital Wuerzburg, Germany	N/A
Chemicals, peptides, and recombinant proteins		
1x PBS	Dulbecco's	PAA; H15-002
2-Mercaptoethanol	Sigma Aldrich	M6250-250ML
2-Propanol	VWR	20839.366
Agarose	Biozym	LE Agarose; 840004
Aquapolymount	Polysciences	18606
B-27 supplement	Gibco	17504–044
BDNF	Homemade; produced in *E. coli*	N/A
Betaine	Sigma Aldrich	61962-250G
Bromophenol blue	Sigma Aldrich	B8026
Chloroform	Sigma Aldrich	32211-2,5L-M
Dithiothreitol (DTT)	Thermo Scientific	20291
Donkey Serum	Merck	S30-100mL
EtBr2	Sigma Aldrich	E8751
EtOH	Honeywell	32205-2,5L
Ethylene glycol	Roth	9516.1
FluorSave Reagent	Merck, Calbiochem	345789-20mL
LR White resin	Electron Microscopy Sciences (Hatfield, PA, USA)	14380
Formaldehyde	Merck	1.04003.1000
Formamide	Sigma Aldrich	F7503-1L
Glucose	Sigmal Aldrich	G6152
Glutamax	Gibco	35050–038
Glutaraldehyde (25%)	SERVA	23114.01
Glycerol	Honeywell	15523-1L
Glycine	Roth	3790.3
HBSS	Thermo Scientific	14170–138
Heparin (25.000 I.U.)	Ratiopharm	N68542.04
Horse serum	Linaris	SHD3250YK
KCl	Roth	6781.1
KH_2PO_4	Merck	1.04873.1000
Laminin	Thermo Scientific	23017–015
Luminaris HiGreen qPCR Master Mix	ThermoFisher	K0991
Methanol	Sigma Aldrich	32213-2.5L-M
$MgCl_2$	Thermo Scientific	F-510MG
Milk powder	Roth	T145.3
Na_2HPO_4	Roth	P030.2
NaCl	Roth	9265.2
NaH_2PO_4 x $2H_2O$	Merck	1.06342.1000

(*Continued on next page*)

Continued

REAGENT or RESOURCE	SOURCE	IDENTIFIER
NaOH (1N)	Merck	1091371000
Neurobasal medium	Thermo Scientific	21103049
Neutravidin beads	Thermo Scientific	29200
Nonident NP-40	Sigma Aldrich	74385-1L
Paraformaldehyde (PFA)	Merck	1.04005.1000
Phosphatase Inhibitor	Roche	04906837001
Poly D-L-Ornithine	Sigma Aldrich	P8638-500MG
Protease Inhibitor	Roche	04693159001
SKF38393	Sigma Aldrich	D047-100MG
Sodium Deoxycholate	Applichem	A1531.0100
SKF81297	Tocris	1447
Oxotremorine M	Tocris	1067
Sodium dodecyl sulfate (SDS)	Applichem	A2572.1000
Sulfo-NHS-SS-Biotin	Thermo Scientific	21331
Tris HCl	Roth	9090.3
Triton X-100	Sigma Aldrich	23472-9 & X100-1L
TRIZMA	Applichem	A1086,1000
Trizol	Invitrogen	15596–026
Trypsin	Worthington	TRL3
Trypsin inhibitor	Sigma Aldrich	T6522-100MG
Tween 20	Sigma Aldrich	P1379-1L
Washing Buffer (Surface Biotinylation)	Thermo Scientific	1859389
Critical commercial assays		
Goat-on-Rodent-AP-Polymer kit	Biocare Medical	GAP514G
Permanent AP Red kit	Zytomed	ZUC001-125
HRP Polymer kit	Zytomed	POLHRP-006
DAB substrate kit	Zytomed	DAB057
RNase free DNase set	Qiagen	79254
Thermo Scientific™ First Strand cDNA Synthesis Kit	Thermo Scientific	K1612
Deposited data		
Unprocessed original data files & statistical data	This paper; Mendeley Data	https://doi.org/10.17632/n4hz94m7yc.1
Experimental models: Organisms/strains		
Rat: Sprague-Dawley rats: Sim:SD	Charles River (Sulzfeld, Germany)	RRID: RGD_10395233
Mouse: C57Bl6/J	Charles River (Sulzfeld, Germany)	RRID: IMSR_JAX:000664
Mouse: FVB/NJ	Charles River (Sulzfeld, Germany)	RRID: IMSR_JAX:001800
Mouse: DRD1-eGFP: *D1-GFP [TG(DRD1a-EGFP)X60Gsat]*	MMRRC	RRID: MMRRC_000297-MU
Mouse: DRD2-eGFP: *D2-GFP [TG(DRD2-EGFP)S118Gsat]*	MMRRC	RRID: MMRRC_000230-UNC
Mouse: DRD1-td-Tomato: *Tg(Drd1a-tdTomato)6Calak*	IMSR	Cat# JAX:016204; RRID: IMSR_JAX:016204
Mouse: TrkB deficient: B6; 129S4-*Ntrk2*^{tm1Rohr}	University of California	RRID: MMRRC_000188-UCD
Mouse: DRD1$^{-/-}$ mice	Dr. Rosario Moratalla, Instituto Cajal, Consejo Superior de Investigaciones Cientificas (CSIC), 28002 Madrid, Spain	N/A

(*Continued on next page*)

Continued

REAGENT or RESOURCE	SOURCE	IDENTIFIER
Oligonucleotides		
Primer for full-length rat-TrkB forward: 5′- GTTGGCGAGACATTCCAAG-3′	This paper	N/A
Primer for ful-length rat-TrkB reverse: 5′- GGGGGTTTTCAATGACAGG-3′	This paper	N/A
Primer for GAPDH forward: 5′-GCAAATTCAACGGCACA-3′	This paper	N/A
Primer for GAPDH reverse: 5′-CACCAGTAGACTCCACGAC-3′	This paper	N/A
Software and algorithms		
Olympus FV10-ASW 3.0 Viewer	Olympus	RRID: SCR_014215
Endnote X9	Endnote	https://endnote.com
GIMP 2.8	GIMP	https://www.gimp.org
GraphPad Prism 6.0	GraphPad	RRID: SCR_002798
ImageJ	ImageJ	RRID: SCR_003070
Microsoft Office	Microsoft	RRID: SCR_016137
Adobe Illustrator software	Adobe	RRID: SCR_010279

RESOURCE AVAILABILITY

Lead contact

Further information and requests for resources and reagents should be directed to and will be fulfilled by the lead contact, Dr. Michael Sendtner (Sendtner_M@ukw.de).

Materials availability

All materials reported in this paper will be shared by the lead contact upon request.

Data and code availability

- The unprocessed microscopic raw data, western blots and an excel file containing detailed information about image processing for each individual image as well as statistical raw data and analyses were uploaded to Mendeley Data: https://data.mendeley.com https://doi.org/10.17632/n4hz94m7yc.1, and are publicly available as of the date of publication. DOIs are listed in the key resources table.
- This paper does not report original code.
- Any additional information required to reanalyze the data reported in this paper is available from the lead contact upon request.

EXPERIMENTAL MODEL AND SUBJECT DETAILS

Animals

Rats

The study was conducted on male Sprague-Dawley rats (RRID: RGD_10395233, 150–175 g at the beginning of the experiments) purchased from Charles River (Sulzfeld, Germany). The rats were kept under controlled environmental conditions (22–24°C; 50–60% humidity; 12 h light/dark cycle; light on at 7:00 a.m.) with free access to standard laboratory chow (Altromin 1324 standard diet; Altromin, Lage, Germany) and water. To avoid social stress, rats were maintained two per cage in transparent Makrolon polycarbonate type III cages (38 × 22 × 20 cm) with nesting material (paper) for environmental enrichment. Transfer to new cages was twice per week. All rats were adapted to the laboratory and habituated to handling for at least five days before starting the experiments.

Mice

Brain tissue was dissected from P1-3, or adult (P56-P84) male & female mice for cell culture or IHC analyses from WT (C57Bl6/J, RRID:IMSR_JAX:000664; FVB/NJ, RRID: IMSR_JAX:001800), DRD1-eGFP mice (*D1-GFP [TG(DRD1a-EGFP)X60Gsat],* RRID: MMRRC_000297-MU), DRD2-eGFP mice (*D2-GFP [TG(DRD2-EGFP)S118Gsat]*, RRID: MMRRC_000230-UNC), DRD1-td-Tomato mice (*Tg(Drd1a-tdTomato)6Calak*, IMSR Cat# JAX:016204, RRID: IMSR_JAX:016204) or P1-5 TrkB deficient *Ntrk2*^{tm1Rohr} mice (MGI Cat# 3040875, RRID: MGI:3040875).

All experiments were approved by a license for animal testing (approval number: 55.2–2531.01 76/11 & 55.2-2532-2-728) and performed in accordance with the supervision through local veterinary authority (Veterinaeramt der Stadt Wuerzburg) and Committee on the Ethics of Animal Experiments, i.e., Regierung von Unterfranken, Wuerzburg, Germany.

Drd1$^{-/-}$ mice were provided by Dr. Rosario Moratalla, Instituto Cajal, Consejo Superior de Investigaciones Cientificas (CSIC), 28002 Madrid, Spain. In this study we used 3–4 months old *Drd1*$^{-/-}$ mice backcrossed with BAC-transgenic mice *Drd2-eGFP* (*Drd*$^{-/-}$*-Drd2-eGFP*)[14,20] and BAC transgenic *Drd1-tomato* mice as control animals. The BAC transgenic mice were used to identify the striatal direct and indirect pathway neurons. All the mice were bred in C57BL/6 background and genotyped by PCR analysis. Mice were housed in groups of 4–6 per cage, with constant room temperature (21–22°C) and 12 h light/dark cycle (lights on at 7:00 h) and were given free access to food and water. All experimental procedures were approved by the Cajal Institute Bioethics Committee and by CSIC Ethics Committee and fulfill the requirements of Spanish (RD 53/2013) and European Union (63/2010/EU) legislation.

Hemiparkinsonian 6-OHDA lesion

Surgery was performed under isoflurane anesthesia (3.5% for initiation, 2% for maintaining) with additional local anesthesia (bupivacaine 0.25%) for the scull. 6-OHDA was dissolved in 0.9% sodium chloride with 0.1% ascorbic acid and was kept on ice. Stereotactic microinjection of 6-OHDA (3.6 mg/mL) was performed targeting the right medial forebrain bundle (MFB; AP-4.4 mm, L-1.2 mm, V-7.8 mm, IB -2.4 mm (2.5 μL) and AP-4.0 mm, L-0.8 mm, V-8.0 mm, IB+3.4 mm (3 μL) according to bregma (Paxinos and Watson). The toxin was injected at a rate of 1μL per minute. After injection the cannula was left in place for another minute and then slowly retracted. At the end of the surgery the animals received an injection of tramadol (12.5 mg/kg) for postoperative analgesia. The treatment was continued in fresh-drinking water (1 mL tramadol in 100 mL water) for two days after surgery. To prevent weight loss, animals had access to soft pellets and standard baby food. Apomorphine rotation test for functional lesion assessment was not performed because apomorphine is a DRD2-agonist and our aim was to investigate effects of complete absence of dopamine receptor activation on TrkB translocation. The success of the 6-OHDA lesion was instead verified by absence of either TH-IR or protein in immunohistochemistry and WB analyses.

Similarly, 7–8-month-old *Drd1-td-Tomato* mice were treated with 6-OHDA injection under isoflurane anesthesia, and 6-OHDA (15 mg/mL) was microinjected targeting the right medial forebrain bundle (MFB); AP-1.2 mm, ML-1.1 mm, DV-5 mm (0.2uL), according to bregma (Paxinos and Watson). Sham controls were performed by vehicle injection in age-matched wild type mice. The toxin or vehicle, respectively, was injected at a rate of 0.1μL per minute. Starting one day after injection, mice were given daily i.p. injections of either Benserazid (12 mg/kg) and L-DOPA (30 mg/kg) or saline. To prevent weight loss, animals had access to soft pellets. Mice were also placed on a warm plate in the first week following injection to prevent hypothermia.

METHOD DETAILS

Cell culture

For primary cell culture striatum of newborn pups (P1-3) was collected in 250μL ice-cold HBSS per animal. Trypsinization was performed with 50μL 1% trypsin for 30 min at 37°C before the reaction was stopped by adding 50μL trypsin-inhibitor. Afterward tissue was collected in a 15mL tube provided with Neurobasal medium (Thermo Scientific; 21103049) containing B27^{TM} supplement (Gibco; 17504-044), Glutamax (Gibco; 35050-038), Penicillin/Streptomycin and Horse Serum. A total of three trituration and centrifugation steps were performed to remove debris and nucleic acids from the cell suspension. For non-sorted primary SPN cultures, cells were then resuspended in an appropriate volume and plated on Polyornithine/Laminin-111-coated cell culture dishes.

Instead of directly plating the cells, cell suspension derived from *Drd1-td-Tomato* mice (*Tg(Drd1a-tdTomato)6Calak*, IMSR Cat# JAX:016204, RRID:IMSR_JAX:016204) were FACS-purified using a BD FACS ARIA III sorter. To ensure specificity, WT and Tg^{+} animals were initially sorted separately. After the sorting setup was optimized to ensure high sorting sensitivity and specificity, tissue from all littermates which include 50% WT was pooled. Cell culture medium was replaced completely to serum-deprived cell culture medium after 24h to prevent any serum-related effect on dopamine receptor or TrkB stimulation. Cell cultures were maintained for 7-21DIV before preparation for ICC or WB (including surface biotinylation).

Stimulation of striatal SPNs

Striatal SPNs were pharmacologically stimulated with the following substances diluted in serum-free cell culture medium (timescale indicated in experiments): BDNF 10 ng/mL (homemade), SKF38393 2μM (Sigma Aldrich; D047-100MG), SKF81297 20μM (Tocris; #1447), Oxotremorine M 10μM (Tocris; #1067), 100nM Bafilomycin (ENZO: BML-CM110-0100). After stimulation, cells were washed with 1xPBS before processing for ICC or WB.

Immunocytochemistry

Cells were fixed and cross-linked with 4% PFA (37°C, pH 7.4) at RT, for 10min and washed twice with 1xPBS. Permeabilization and blocking were performed in 1xPBS, 10% Donkey serum, 0.1% Triton X-100 at RT for 1h. Primary antibodies were incubated in permeabilization and blocking solution at 4°C o.n. Cells were then washed in 1xPBS, 0.1% Triton X-100 and secondary antibodies were incubated for 1h. Nuclei were stained with 0.4 μg/mL 4′,6-diamidino-2-phenylindole (DAPI). Cells were mounted on

Superfrost®Plus glass slides (25 × 75 × 1.0mm Thermo Fisher Scientific; #J1800AMNZ) using MERCK-FluorSave reagent (Merck; #345789-20ML).

Cylinder test

As a test for altered motor function in 6-OHDA treated mice, spontaneous forepaw use was analyzed using the cylinder test both prior and two weeks after 6-OHDA injection. Mice were placed in a transparent cylinder of 12cm diameter and 30cm height in front of two mirrors and recorded for 12 min. The number of touches on the inner surface of the cylinder with either the ipsilateral or contralateral paw was then assessed. Data shown represent the percentage of ipsilateral forepaw touches relative to pre-OP measurements.

Preparation of tissue for immunostaining

Rats or mice were deeply anesthetized with 120 mg/kg ketamine hydrochloride and 16 mg/kg xylazine hydrochloride in 0.4–0.6mL 1xPBS and transcardially perfused through the left ventricle. Blood vessels were flushed with 1xPBS, 0.4% Heparin for 2-3min. Fixative perfusion was performed with 4% PFA, pH 6.0–7.4 in Phosphate Buffer for ~8min (mice) or 12min. (rats). Subsequently, brains were removed from the skull and allowed for post-fixation in 4% PFA at 4°C for 0.5h (mice) or o.n. (rats). Mouse pups (P1-5) were not perfused, but brains were incubated in 4% PFA at 4°C for 8-12h o.n. Brains were then washed in 1xPBS and embedded in 6% agarose. 20-40μm free-floating, coronal brain sections were obtained, using a LEICA Vibratome VT1000S (RRID:SCR_016495) and stored in "Cryoprotection Anti-Freeze Buffer" (1xPBS, Glycerol, Ethylene glycol) at −20°C.

D1R-deficient animals were anesthetized with pentobarbital (50 mg/kg, i.p.) and then perfused with 4% paraformaldehyde dissolved in PB (phosphate buffer, pH 7.4), dissected and immersed overnight in the same fixative. Brains were sectioned in 30μm thick coronal slices at the vibratome and kept in PBS until used.[91]

Immunohistochemistry – Rat and mouse

Free-floating vibratome sections were washed in 1xPBS. Blocking and permeabilization were performed as one step using 1xPBS, 0.3% Triton X-100, 0.1% Tween 20, and 10% normal Donkey serum for 2h. Primary antibodies were diluted in permeabilization and blocking buffer and incubated at a final concentration between 0.5 and 1.0 μg/mL in the presence of 0.01% NaN_3 on a shaker at 4°C for 72h. Afterward, the slices were washed in 1xPBS, 0.1% Triton X-100, 0.3% Tween 20. Secondary antibodies were diluted in permeabilization and blocking buffer at a final concentration of 0.625 μg/mL. After secondary antibody incubation, the brain slices were extensively washed with 1xPBS, 0.1% Triton X-100, 0.3% Tween 20. Nuclei were stained with 0.4 μg/mL 4′,6-diamidino-2-phenylindole (DAPI). After DAPI incubation, sections were washed twice in 1xPBS before they were rinsed in dH_2O and finally mounted on SuperfrostPlus glass slides (25 × 75 × 1.0mm Thermo Fisher Scientific; #J1800AMNZ) using MERCK-FluorSave reagent (Merck; #345789-20ML).

Proteinase K treatment of 6-OHDA rat brain sections

To analyze the formation of insoluble TrkB or Pan-Trk aggregates (Figure 5), 40μm free floating vibratome sections of PFA-fixed hemiparkinsonian rats were digested with 10 μg/mL proteinase K (PK) (Invitrogen, no. 4333793) in 1xPBS pH7.4 at 55°C for 15min. using a previously published protocol.[71,72] Control sections were incubated in 1xPBS without PK at 55°C for 15min. After PK treatment, sections were immediately washed with ice-cold 1xPBS followed by permeabilization & blocking in 1xPBS, 10% DS, 0.3% Triton X-100, 0.1% Tween 20. Further steps were performed according to normal IHC in mice and rats, described above. To visualize potentially insoluble aggregates, digested sections and controls were double stained against TrkB or Pan-Trk, together with the cytosolic SPN marker DARPP-32, Tyrosine-hydroxylase (TH) to identify the DA-depleted striatal hemisphere and GM130 as a marker for a membrane-surrounded compartment. Complete absence of DARPP-32, TH or GM130-IR indicated successful PK digestion.

Immunohistochemistry – Human postmortem tissue

Human postmortem tissue derived from either patients with PD or controls who died by a non-neurological condition was de-paraffinated followed by boiling in citrate buffer (pH6.0) for 10min. Tissue was then rinsed in TBS (pH7.6), followed by H_2O_2 block for 15min. and another rinsing step in TBS. DARPP-32 (R&D Systems, AF6259) was diluted 1:200 in TBS, 3% BSA and was incubated at RT for 3h. DARPP-32 was stained using Goat-on-Rodent-AP-Polymer kit (Biocare Medical #GAP514G) and Permanent AP Red kit (Zytomed #ZUC001-125). Afterward, panTrk (Abcam [EPR17341], ab181560) was diluted 1:50 in TBS, 3% BSA and was incubated on brain tissue for 48h. panTrk was stained using an HRP Polymer kit (Zytomed# POLHRP-006) and DAB substrate kit (Zytomed #DAB057). Nuclei were stained for 2min., using hematoxylin. Tissue was finally dehydrated, rinsed in xylol, and embedded in Mowiol or MERCK-FluorSave reagent (Merck; #345789-20ML).

Correlative light and electron microscopy (CLEM)

Brain sections from hemiparkinsonian rats

CLEM was performed after finishing the IHC protocol (rats and mice) using free-floating vibratome brain sections (30-50μm) and rhodamine-based secondary antibodies. These were embedded in LR White resin, and the CLEM workflow was performed according to previously published protocols.[92–94] Semi-thin resin sections (200 nm) were transferred onto a poly-L-lysine-coated microscopy slide and nuclei were stained with Hoechst for 10 min. Sections were mounted in Mowiol and high-precision coverslips.

Fluorescence images were acquired using the Elyra S.1 SIM (Zeiss, Germany). The samples were then processed for imaging at the SEM by removing the coverslips, washing off the mounting medium and contrasting with heavy metals as follows: the sections were first incubated in 2.5% uranyl acetate in ethanol for 15min and in 50% lead citrate in H_2O for 10 min[95] Carbon coating was performed with the Compact Coating Unit CCU-010 (Safematic, Bad Ragaz, Switzerland) resulting in ~3 nm coating. Images were taken with the JSM-7500F scanning electron microscope (JEOL USA, Inc., Peabody, MA USA).

Registration of the fluorescence and electron microscopy images was accomplished with Inkscape 0.91 (Inkscape Community) using the heterochromatin pattern as an intrinsic landmark. For an unbiased correlation, the channel of interest was hidden and only the DNA signal was used. After the correlation the channel of interest was revealed, and all channels were merged.

Microscopy

Coronal brain slices were analyzed with an Olympus FluoView 1000 confocal laser microscope equipped with the following objectives: 10× (NA: 0.25), 20x (NA: 0.75), 40x (oil differential interference contrast, NA: 1.30) or 60x (oil differential interference contrast, NA: 1.35). Images were obtained with the corresponding Olympus FV10-ASW (RRID: SCR_014215) imaging software for visualization and image acquisition in a single channel scan mode as z-stacks, using 405nm, 473nm, 559nm, and 633nm lasers. The resulting images (Olympus.oib format) were processed using ImageJ (RRID: SCR_003070) and projected as either maximum or average intensity. Super resolution images were obtained with a Zeiss Elyra S.1 structural illumination microscopic (SIM) setup and Zeiss "ZEN 2.1 SP-1″ image acquisition software. dSTORM super resolution images were obtained as described before.[96,97] Electron microscopy images were obtained with a JSM-7500F scanning electron microscope (JEOL USA, Inc., Peabody, MA USA).

Brightness and contrast were modified in accordance with general rules of good scientific practice and all changes were monitored and documented for each experiment and each image. The gamma correction was not changed in any case. Finally, the data were transferred into png format, arranged with Adobe Illustrator software (RRID: SCR_010279) and saved as 300dpi png and tif files.

Quantification of TrkB/SORCS-2 co-localization

Quantification of TrkB / SORCS-2 co-localization in soma versus peripheral neurites of FACS-enriched dSPNs was performed using ImageJ – Coloc-2 tool. A Multi ROI was created covering the somatic area of dSPNs. Afterward co-localization was calculated between the TrkB channel, and the SORCS-2 channel as Pearson's R value (no threshold). At the same time true co-localization was confirmed by documentation of the Costes-P value > 0.95 to determine true co-localization of up to 3%.[98] Afterward, the somatic ROI was deleted from both channels and co-localization measurement was repeated for the neurites. All values were indicated in percent. Finally, a ratio of TrkB/SORCS-2 co-localization was calculated by dividing neurite co-localization by somatic co-localization. Values > 1 indicated higher co-localization in neurites versus soma, while values < 1 indicate higher co-localization in the cell body.

Quantification of TrkB-associated Lamp-1 positive lysosomes

For quantification of TrkB presence in lysosomal structures, the number of Lamp-1 positive structures was counted manually by the experimenter. Afterward, the number of lysosomes that contained TrkB-IR was counted. Finally, the amount of TrkB-positive lysosomal structures was calculated in percent of all lysosomal structures.

Western blot analyses

Tissue preparation for western blot analysis

Rats or mice were euthanized with CO_2 before decapitation. Newborn mice (P1-5) were anesthetized on ice before decapitation. The brains were removed and transferred to either ice-cold 1xPBS or 1x HBSS. The striatum was dissected and immediately frozen in liquid N_2. Tissue was lysed in 0.05M Tris pH7.5, 0.15M NaCl, 1% NP-40, 0.5% Sodiumdeoxychelate, 0.1% SDS containing protease inhibitor (Roche #11697498001 or 11836153001) and phosphatase inhibitor (Roche; #04906837001). A Hielscher sonifyer was used for tissue lysis. Samples were then subjected to 30min. centrifugation at 20.000xg (4°C) and supernatants were collected. Protein content was measured, using a Pierce Protein Research BCA kit (Thermo Scientific #23225) or Bradford Assay (Bio Rad # 5000201). Either 30 or 40μg of protein were diluted in Laemmli buffer and boiled at 99°C for 5min. before being applied to 5–9% PAA gradient-gels.

Cell culture - Surface biotinylation assay

Surface biotinylation was performed using the Pierce Surface biotinylation kit (Thermo Scientific; 89881). Each cell culture provided 20μL Input, 180μL Flow Through (intracellular fraction) and 100μL Pull Down (surface fraction). Samples were diluted 1:1 in 2x Laemmli buffer, before a quick sonication was performed. Samples were then heated to 95–99°C for 5min. followed by 1min 20.000xg and loading on PAA gels (5–9% gradient).

TrkB Immunoprecipitation

3μg Rabbit anti TrkB (Millipore Cat# 07–225, RRID: AB_310445) and 30μL protein A agarose were diluted in 0.05M Tris HCl (pH7.5), 0.15M NaCl, 1% Nonident NP-40, 0.05% Sodium Deoxycholate with protease and phosphatase inhibitor (IP-lysis/wash buffer-1) and incubated at 4°C for 2h. 300μg striatal protein lysate of either P5 WT-control or *Ntrk2*^{tm1Rohr} mice was added and incubated at 4°C o.n. in a rotation wheel. The next day samples were centrifuged at 1000xg for 1min. and the supernatant was saved as the "Flow Through" fraction. Beads were washed twice with wash buffer-1 (20min. each at 4°C in a rotation wheel). Afterward, beads were washed once in 0.05M Tris HCl (pH7.5), 0.5M NaCl, 0.1% Nonident NP-40, 0.05% Sodium Deoxycholate, proteinase and

phosphatase inhibitor. Final washing step was performed in 0.01M Tris HCl (pH7.5), 0.1% NP-40, 0.05% Sodium Deoxycholate. 30μL 2xLaemmli buffer were added to beads followed by heating to 99°C for 5min. Samples were then either used for gel electrophoresis or stored at −20°C.

Gel electrophoresis and detection

Gel electrophoresis for either surface biotinylation samples or tissue-derived samples was performed in 1x Electrophoresis buffer (25mM Tris, 0.2M Glycine, 0.1% SDS, in dH2O, pH 8.35) at U = 120V const.; I∼20mA per gel. After the gel run samples were blotted (Wet-Blotting) on PVDF membranes at U = 120V, I = 0.35A, p = 50W for 60min. PVDF membranes were blocked with 1xTBST, 5% Milk powder and proteins were detected using the indicated primary antibodies diluted in 1xTBST, 0.02% NaN_3 followed by incubation with POD-linked secondary antibodies. Chemiluminescence was detected with ECL Western Blotting Detection kit (Millipore® Immobilon Western HRP Substrate Luminol Reagent #WBKLS0500). After detection, HRP was inactivated by washing 15min. in 1xTBST, 0.1% NaN_3, followed by extensive rinsing in 1xTBST before applying further primary antibody incubation.

Quantification of pTrk induction in FACS SPNs

Band intensities were measured with ImageJ and pTrk was normalized to Calreticulin. Alterations in pTrk inducibility by BDNF after pharmaceutical stimulation of DRD1 in dSPNs were calculated as percent of the pTrk signal evoked by BDNF alone, without any pharmaceutical stimulation.

Quantification of TrkB surface expression levels in FACS SPNs

Band intensities were measured with ImageJ and TrkB in the "Pull Down" fraction was normalized to Calreticulin. Alterations in TrkB cell surface expression after pharmaceutical stimulation of DRD1 in dSPNs were calculated as percent of the TrkB Pull Down fraction in unstimulated control.

Quantification of protein levels in 6-OHDA rat striatum

Band intensities were measured with ImageJ and were normalized to loading control Calreticulin.

RNA purification from tissue and RT-PCR

For RNA extraction from tissue, intact and 6-OHDA lesioned rat striatum was dissected and frozen in liquid N_2. Purification of RNA from tissue was performed according to the original protocol, using a Trizol-lysis, based on acidic guanidinium thiocyanate - phenol - chloroform extraction, described by Chomczynski and Sacchi.[99] RNA contained in the aqueous phase was precipitated with isopropanol, washed three times with 70% EtOH and finally dissolved in 50μL RNAse-free H_2O. Genomic DNA was digested using a RNase-free DNase set (Qiagen, #79254). RNA concentration was measured with a Nanodrop Spectrophotometer (Peqlab; ND-1000, RRID:SCR_016517). 500ng purified RNA was used for reverse transcriptase-mediated cDNA synthesis, using the Thermo Scientific™ First Strand cDNA Synthesis Kit (#K1612). cDNA was diluted 1:5 in RNase-free H_2O and 2μL cDNA were used for qRT-PCR using a Roche LightCycler® 96 with the following primers against full-length rat-TrkB (forward: 5′- GTTGGC GAGACATTCCAAG-3′; reverse: 5′- GGGGGTTTTCAATGACAGG-3′) and GAPDH (forward: 5′-GCAAATTCAACGGCACA-3′; reverse: 5′-CACCAGTAGACTCCACGAC-3′). Results were exported to Microsoft Excel and analyzed with GraphPad Prism 6.0 for statistical analysis. TrkB mRNA values were normalized to GAPDH and TrkB mRNA levels were calculated in percent of mean TrkB mRNA levels in intact striatum.

QUANTIFICATION AND STATISTICAL ANALYSIS

The number of experiments was designed at the planning stage, based on numbers of independent experiments that are commonly used for these types of experiments in this research field. All datasets were analyzed for normality by Shapiro-Wilk test. Afterward t test was performed between pairs (normal distribution) or one sample t test if a control group was set to 100% for comparison. For more than two groups One/two-way ANOVA and Tukey multiple comparison test (normal distribution), or Kruskal-Wallis, Mann Whitney, or Friedman test (no normal distribution) was performed, using GraphPad Prism software. The type of statistical test is indicated in each figure.